

Construction and application of an algebraic dual basis and the Fine-Scale Greens' Function for computing projections and reconstructing unresolved scales

Shrestha, Suyash; Dekker, Joey; Gerritsma, Marc; Hulshoff, Steven; Akkerman, Ido

DOI

[10.1016/j.cma.2024.116833](https://doi.org/10.1016/j.cma.2024.116833)

Publication date

2024

Document Version

Final published version

Published in

Computer Methods in Applied Mechanics and Engineering

Citation (APA)

Shrestha, S., Dekker, J., Gerritsma, M., Hulshoff, S., & Akkerman, I. (2024). Construction and application of an algebraic dual basis and the Fine-Scale Greens' Function for computing projections and reconstructing unresolved scales. *Computer Methods in Applied Mechanics and Engineering*, 422, Article 116833. <https://doi.org/10.1016/j.cma.2024.116833>

Important note

To cite this publication, please use the final published version (if applicable).
Please check the document version above.

Copyright

Other than for strictly personal use, it is not permitted to download, forward or distribute the text or part of it, without the consent of the author(s) and/or copyright holder(s), unless the work is under an open content license such as Creative Commons.

Takedown policy

Please contact us and provide details if you believe this document breaches copyrights.
We will remove access to the work immediately and investigate your claim.



Construction and application of an algebraic dual basis and the Fine-Scale Greens' Function for computing projections and reconstructing unresolved scales

Suyash Shrestha ^{a,c,*}, Joey Dekker ^{b,c}, Marc Gerritsma ^c, Steven Hulshoff ^c, Ido Akkerman ^d

^a ETSIAE-UPM-School of Aeronautics, Universidad Politécnica de Madrid, Plaza del Cardenal Cisneros 3, Madrid, E-28040, Spain

^b Delft University of Technology, Delft Institute of Applied Mathematics, Mekelweg 4, Delft, 2628 CD, The Netherlands

^c Delft University of Technology, Faculty of Aerospace Engineering, Kluyverweg 1, Delft, 2629 HS, The Netherlands

^d Delft University of Technology, Faculty of Mechanical Engineering, Mekelweg 2, Delft, 2628 CD, The Netherlands

ARTICLE INFO

Keywords:

Duality
Projection
Variational multiscale
(Fine-Scale) Greens' function
Poisson equation
Advection–diffusion equation

ABSTRACT

In this paper, we build on the work of Hughes and Sangalli (2007) dealing with the explicit computation of the Fine-Scale Greens' function. The original approach chooses a set of functionals associated with a projector to compute the Fine-Scale Greens' function. The construction of these functionals, however, does not generalise to arbitrary projections, higher dimensions, or Spectral Element methods.

We propose to generalise the construction of the required functionals by using dual functions. These dual functions can be directly derived from the chosen projector and are explicitly computable. We show how to find the dual functions for both the L^2 and the H_0^1 projections. We then go on to demonstrate that the Fine-Scale Greens' functions constructed with the dual basis functions consistently reproduce the unresolved scales removed by the projector.

The methodology is tested using one-dimensional Poisson and advection–diffusion problems, as well as a two-dimensional Poisson problem. We present the computed components of the Fine-Scale Greens' function, and the Fine-Scale Greens' function itself. These results show that the method works for arbitrary projections, in arbitrary dimensions. Moreover, the methodology can be applied to any Finite/Spectral Element or Isogeometric framework.

1. Introduction

The origin of the Variational Multiscale (VMS) method stems from the series of papers on stabilisation techniques for finite-element methods found in [1–10] along with [11]. The VMS methodology itself was first introduced in [12] as a re-interpretation of the SUPG formulation where it was shown that stabilisation methods could be derived from a solid theoretical foundation. Fundamentally, the multiscale framework entails incorporating the missing unresolved/fine-scale effects into the numerically computed large/resolved scales such that the numerical solution becomes the chosen projection of the exact solution. Moreover, it has served as a fundamental basis for the development of stabilised methods for applications such as turbulence modelling in the context of Large Eddy Simulation (LES), see [13–17]. Other examples include [18–22] where VMS is employed for performing LES in

* Corresponding author at: ETSIAE-UPM-School of Aeronautics, Universidad Politécnica de Madrid, Plaza del Cardenal Cisneros 3, Madrid, E-28040, Spain.
E-mail addresses: s.shrestha-1@tudelft.nl, s.shrestha@upm.es (S. Shrestha).

Discontinuous Galerkin and Isogeometric frameworks, along with [23] wherein Discontinuity Capturing is tackled using multiscale theory.

A key ingredient for formulating the VMS approach is the so-called *Fine-Scale Greens' function*, which was first introduced in [24] and was formally characterised in [25]. More specifically, in [25] the explicit construction of the Fine-Scale Greens' function is demonstrated using the classic Greens' function and the choice of a projector. Although a general derivation of the Fine-Scale Greens' function is presented the actual construction for the Fine-Scale Greens' function for arbitrary projections in arbitrary dimensions is not entirely generalised. This is because the construction of the functionals associated with the projector, referred to as μ 's in [25], is not clarified for general cases.

In the present work, we seek to build on [25] by proposing a set of μ 's which is unique for every projector and generalises to arbitrary dimensions. To achieve this, we propose using a new set of basis functions, namely dual basis functions, to act as the μ 's. This enables the explicit construction of the Fine-Scale Greens' function for any given projector in arbitrary dimensions using the classic Greens' function. To start off, we briefly present a review of the work from [25] in Section 2. Subsequently, we present a discussion on the Mimetic Spectral Element Method (MSEM) and the associated primal and dual function spaces in Section 3. In this section, we also highlight the link between the chosen projector and the dual basis functions. Note that while we work with the MSEM throughout this study, the concepts are by no means limited to the MSEM. The presented work can be extended to Finite/Spectral Element or Isogeometric approaches by simply evoking the concept of duality introduced in this paper.

In Section 4 we move on to construct the Fine-Scale Greens' function associated with the H_0^1 and L^2 projections for the 1D Poisson equation. Here we perform several numerical tests to demonstrate that the constructed Fine-Scale Greens' functions can exactly reconstruct all the fine scales truncated by the projection. Furthermore, we also show how the Fine-Scale Greens' function for the Poisson problem may be used in an advection–diffusion problem to reconstruct the corresponding fine scales. Although this involves solving coupled sets of equations instead of a direct computation, it overcomes the complexity of dealing with the classical Greens' function of the advection–diffusion problem. We close in Section 5 by presenting the methodology applied to the 2D Poisson problem to demonstrate the generalisation to higher dimensions.

2. Hughes and Sangalli approach

The theory of variational multiscale analysis that this work builds upon was presented by Hughes and Sangalli in [25]. This section serves as a brief review of the original work of [25] where we lay down the fundamental concepts for formulating the VMS approach. First, the continuous setup is reviewed, followed by the finite-dimensional setting.

2.1. Continuous case

In [25, §2], the following problem is considered. Let V be a Hilbert space with a norm $\|\cdot\|_V$ and a scalar product $(\cdot, \cdot)_V$. Let V^* be the dual of V , with ${}_{V^*}\langle \cdot, \cdot \rangle_V$ the duality pairing between V^* and V . Let $\mathcal{L} : V \rightarrow V^*$ be a linear isomorphism. The problem can then be stated as: given $f \in V^*$, find $u \in V$ such that

$$\mathcal{L}u = f. \quad (1)$$

The variational formulation of (1) reads as: find $u \in V$ such that

$${}_{V^*}\langle \mathcal{L}u, v \rangle_V = {}_{V^*}\langle f, v \rangle_V \quad \forall v \in V. \quad (2)$$

The solution u is formally expressed as $u = \mathcal{G}f$, with the Greens' operator $\mathcal{G} : V^* \rightarrow V$, that is $\mathcal{G} = \mathcal{L}^{-1}$. This formal problem may also be formulated in a variational multiscale setting. In order to do so, one introduces \bar{V} as a closed subspace of V , along with a linear projector $\mathcal{P} : V \rightarrow \bar{V}$ with $\mathcal{P}^2 = \mathcal{P}$ and $\text{Range}(\mathcal{P}) = \bar{V}$. \mathcal{P} is assumed continuous in V . For the additional formal details, such as the required inf-sup conditions, see [25]. Then, defining $V' = \text{Ker}(\mathcal{P})$, which is a closed subspace of V , combined with the continuity of \mathcal{P} gives

$$V = \bar{V} \oplus V'. \quad (3)$$

This split implies that any $v \in V$ can be uniquely written as $v = \bar{v} + v'$ with $\bar{v} \in \bar{V}$ and $v' \in V'$. In the VMS approach, \bar{V} represents the resolvable coarse scales, while V' represents the unresolved fine scales. When using a VMS approach, one obtains $\bar{u} = \mathcal{P}u$ as the solution for (1), i.e. the numerical error equals the interpolation error and not a multiple of the interpolation error which is usually the case for optimal Finite Element methods. Using (3), the variational formulation from (2) can be split into

$$\begin{cases} {}_{V^*}\langle \mathcal{L}\bar{u}, \bar{v} \rangle_V + {}_{V^*}\langle \mathcal{L}u', \bar{v} \rangle_V &= {}_{V^*}\langle f, \bar{v} \rangle_V \quad \forall \bar{v} \in \bar{V}, & (a) \\ {}_{V^*}\langle \mathcal{L}\bar{u}, v' \rangle_V + {}_{V^*}\langle \mathcal{L}u', v' \rangle_V &= {}_{V^*}\langle f, v' \rangle_V \quad \forall v' \in V'. & (b) \end{cases} \quad (4)$$

These equations are assumed to be well-posed for $\bar{u} \in \bar{V}$ given u' and f , and for $u' \in V'$ given \bar{u} and f , respectively.

As for the non-split formulation in (2), a Greens' operator can also be associated with the split formulation. In particular, the Greens' operator associated with the fine-scale equation in (4) is the *Fine-Scale Greens' operator* $\mathcal{G}' : V^* \rightarrow V'$. This gives u' from the coarse-scale residual $\mathcal{R}\bar{u} = f - \mathcal{L}\bar{u}$,

$$u' = \mathcal{G}'(f - \mathcal{L}\bar{u}) = \mathcal{G}'\mathcal{R}\bar{u}. \quad (5)$$

With \mathcal{G}' , one can eliminate u' from (4) and obtain the VMS formulation for \bar{u} as

$${}_{V^*}\langle \mathcal{L}\bar{u}, \bar{v} \rangle_V - {}_{V^*}\langle \mathcal{L}\mathcal{G}'\mathcal{L}\bar{u}, \bar{v} \rangle_V = {}_{V^*}\langle f, \bar{v} \rangle_V - {}_{V^*}\langle \mathcal{L}\mathcal{G}'f, \bar{v} \rangle_V \quad \forall \bar{v} \in \bar{V}. \quad (6)$$

As a consequence of (3), (6) admits the unique solution $\bar{u} = \mathcal{P}u$.

The above formulation can be used to obtain \bar{u} , but requires obtaining the Fine-Scale Greens' operator \mathcal{G}' . It turns out (see [25, §2.3]) that this operator can be expressed in terms of the full Greens' operator, the projection, and the adjoint projection $\mathcal{P}^T : \bar{V}^* \rightarrow V^*$ which is defined as

$${}_{V^*}\langle \mathcal{P}^T \bar{\mu}, v \rangle_V = {}_{\bar{V}^*}\langle \bar{\mu}, \mathcal{P}v \rangle_{\bar{V}} \quad \forall v \in V, \bar{\mu} \in \bar{V}^*, \quad (7)$$

where \bar{V}^* is the dual space of \bar{V} and ${}_{\bar{V}^*}\langle \cdot, \cdot \rangle_{\bar{V}}$ the pairing between them.

The Fine-Scale Greens' operator is then computed by considering a constrained version of (5) as follows

$$\mathcal{L}u' + \mathcal{P}^T \bar{\lambda} = \mathcal{R}\bar{u} \quad (8)$$

$$\mathcal{P}u' = 0, \quad (9)$$

where the newly introduced $\bar{\lambda} \in \bar{V}^*$ constrains u' to live in the V' space. Given the invertibility of \mathcal{L} , we may write

$$u' = \mathcal{G}(\mathcal{R}\bar{u} - \mathcal{P}^T \bar{\lambda}), \quad (10)$$

which when substituted into (9) and rearranged for $\bar{\lambda}$ gives

$$\bar{\lambda} = (\mathcal{P}\mathcal{G}\mathcal{P}^T)^{-1} \mathcal{P}\mathcal{G}\mathcal{R}\bar{u}. \quad (11)$$

The fine-scale operator \mathcal{G}' can now be expressed in terms of \mathcal{G} and \mathcal{P} as

$$\mathcal{G}' = \mathcal{G} - \mathcal{G}\mathcal{P}^T(\mathcal{P}\mathcal{G}\mathcal{P}^T)^{-1}\mathcal{P}\mathcal{G}, \quad (12)$$

with the properties

$$\mathcal{G}'\mathcal{P}^T = 0, \quad \text{and} \quad \mathcal{P}\mathcal{G}' = 0. \quad (13)$$

See [25, p. 542] for the proof. (12) can be used in (6) to obtain

$${}_{V^*}\langle \mathcal{L}\bar{u}, \bar{v} \rangle_V - {}_{V^*}\langle \mathcal{L}\mathcal{G}'\mathcal{L}\bar{u}, \bar{v} \rangle_V = {}_{\bar{V}^*}\langle (\mathcal{P}\mathcal{G}\mathcal{P}^T)^{-1}\bar{u}, \bar{v} \rangle_{\bar{V}}, \quad (14)$$

which, since $(\mathcal{P}\mathcal{G}\mathcal{P}^T)^{-1}$ is invertible, confirms that (6) is well-posed.

2.2. Finite-dimensional case

In the interest of practical implementations, \bar{V} is a finite-dimensional subspace of V and we seek a set of functionals $\mu \in \bar{V}^*$ which act as the basis for the projection \mathcal{P} . For an N dimensional subspace \bar{V} we seek N functionals which satisfy

$${}_{V^*}\langle \mu_i, v \rangle_V = 0 \quad \forall v \in V' \quad \forall i = 0, 1, \dots, N-1, \quad (15)$$

which in turn implies that $\mathcal{P}v = 0 \quad \forall v \in V'$. These μ 's form a basis for the range of \mathcal{P}^T and we have

$$\mathcal{G}'\mu_i = 0 \quad \forall i = 0, 1, \dots, N-1 \quad (16)$$

$${}_{V^*}\langle \mu_i, \mathcal{G}'v \rangle_V = 0 \quad \forall v \in V^* \quad \forall i = 0, 1, \dots, N-1, \quad (17)$$

following (13). Furthermore, the μ 's may be represented as a vector $\mu \in (\bar{V}^*)^N$

$$\mu = \begin{bmatrix} \mu_0 \\ \mu_1 \\ \vdots \\ \mu_{N-1} \end{bmatrix} \quad \text{and} \quad \mu^T = [\mu_0, \mu_1, \dots, \mu_{N-1}], \quad (18)$$

through which $\mathcal{G}\mu^T \in V^N$, $\mu\mathcal{G}\mu^T \in \mathbb{R}^{N \times N}$ and $\mu\mathcal{G}$ can be written as

$$\mathcal{G}\mu^T = [\mathcal{G}\mu_0, \mathcal{G}\mu_1, \dots, \mathcal{G}\mu_{N-1}] \quad (19)$$

$$\mu\mathcal{G}\mu^T = \begin{bmatrix} {}_{V^*}\langle \mu_0, \mathcal{G}\mu_0 \rangle_V & \dots & {}_{V^*}\langle \mu_0, \mathcal{G}\mu_{N-1} \rangle_V \\ \vdots & \ddots & \vdots \\ {}_{V^*}\langle \mu_{N-1}, \mathcal{G}\mu_0 \rangle_V & \dots & {}_{V^*}\langle \mu_{N-1}, \mathcal{G}\mu_{N-1} \rangle_V \end{bmatrix} \quad (20)$$

$$\mu\mathcal{G}(v) = \begin{bmatrix} {}_{V^*}\langle \mu_0, \mathcal{G}v \rangle_V \\ \vdots \\ {}_{V^*}\langle \mu_{N-1}, \mathcal{G}v \rangle_V \end{bmatrix} \quad \forall v \in V^*. \quad (21)$$

The Fine-Scale Greens' function from (12) may now be rewritten as

$$\mathcal{G}' = \mathcal{G} - \mathcal{G}\mu^T [\mu\mathcal{G}\mu^T]^{-1} \mu\mathcal{G}. \quad (22)$$

In theory, we are free to choose any set of μ which satisfy (15), (16), and (17). In [25] several definitions for μ are proposed for obtaining the Fine-Scale Greens' function for the H_0^1 and L^2 projections of specific example problems. However, their generalisation for arbitrary projections or high-order spectral elements is not considered. This is precisely the knowledge gap that the present work attempts to fill. As such, we turn our attention to constructing a general definition for μ . Naturally, the choice of μ depends on the projection as stated in (15). Ideally, we want a generalised approach for defining the μ corresponding to an arbitrary projector which then consequently yields a unique Fine-Scale Greens' function associated with that projection. To achieve this, we propose the use of dual basis functions.

3. Primal and Dual bases

The dual basis functions considered here were initially created in the context of the Mimetic Spectral Element Method (MSEM) [26]. These are dual functions in the L^2 -sense. In order to understand their link to projections and the use of dual basis functions as the μ 's, we first introduce the primal basis functions and their corresponding L^2 duals. For a more detailed exposition and the extensions to multiple dimensions, see [26].

3.1. Primal basis

A primal basis for nodal functions is constructed based on nodal degrees of freedom. Given such degrees of freedom, denoted by \mathcal{N}_j^0 , the primal basis functions, denoted by $\psi_i^{(0)}$, should satisfy the following property

$$\mathcal{N}_j^0(\psi_i^{(0)}) = \delta_{ij}. \quad (23)$$

We consider the MSEM which uses the Gauss–Legendre–Lobatto (GLL) nodes for nodal degrees of freedom. To define the GLL-nodes, consider the interval $K = [-1, 1] \subset \mathbb{R}$ and let $\xi_i \in K, i = 0, \dots, p$ be the roots of the polynomial $(1 - \xi^2) L_p'(\xi)$, where $L_p(\xi)$ is the Legendre polynomial of degree p and $L_p'(\xi)$ its derivative. The GLL-nodes are then used to define basis functions that satisfy (23) with $\mathcal{N}_j^0(f) := f(\xi_j)$

$$\psi_i^{(0)}(\xi) := \prod_{\substack{j=0 \\ j \neq i}}^p \frac{\xi - \xi_j}{\xi_i - \xi_j}, \quad i = 0, 1, \dots, p. \quad (24)$$

The basis functions $\psi_i^{(0)}(\xi), i = 0, \dots, p$ span the finite dimensional subspace \bar{V} . An example of these basis functions for $p = 3$ is shown in Fig. 1(a).

Next to the basis functions for nodal functions, the MSEM also defines basis functions based on edge degrees of freedom. These are histopolant basis functions based on integral degrees of freedom, defined as

$$\mathcal{N}_j^1(g) = \int_{\xi_{j-1}}^{\xi_j} g(\xi) d\xi, \quad i = 1, \dots, p, \quad (25)$$

where \mathcal{N}_j^1 is a linear functional which extracts integral values from any function $g(\xi)$.

As with the nodal basis, in order to define an edge basis, one looks for basis functions, now denoted $\psi_i^{(1)}$, that satisfy

$$\mathcal{N}_j^1(\psi_i^{(1)}) = \int_{\xi_{j-1}}^{\xi_j} \psi_i^{(1)}(\xi) d\xi = \delta_{ij}. \quad (26)$$

The edge basis functions on the GLL-grid can be expressed in terms of the nodal basis as [27]

$$\psi_i^{(1)}(\xi) := - \sum_{k=0}^{i-1} \frac{d\psi_k^{(0)}}{d\xi}, \quad i = 1, 2, \dots, p. \quad (27)$$

An example of these basis functions for $p = 3$ is shown in Fig. 1(b). Note that the space spanned by these edge functions is the space of polynomials of degree $(p - 1)$.

Remark 3.1. All subsequent references to edge polynomials denoted with degree p refer to a polynomial basis of degree $(p - 1)$.

3.2. Dual basis

Based on the primal basis introduced in the previous section, one can derive an associated dual basis. Before doing so, we first review the definition of a dual space.

Definition 3.1 ([28]). A linear functional α defined on a vector space \mathcal{E} is a real-valued linear function that is a mapping $\alpha : \mathcal{E} \rightarrow \mathbb{R}$

$$\alpha(au + bv) = a\alpha(u) + b\alpha(v), \quad \forall u, v \in \mathcal{E} \text{ and } \forall a, b \in \mathbb{R}. \quad (28)$$

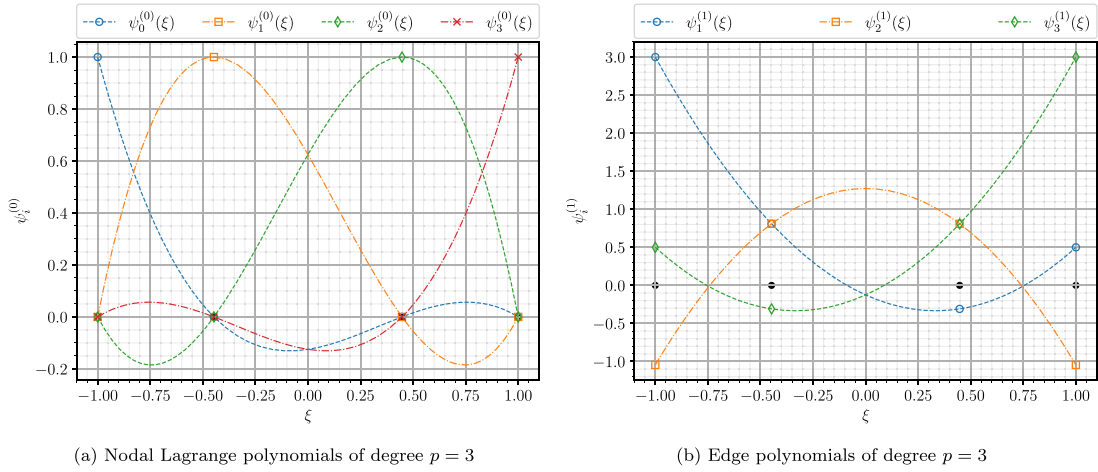


Fig. 1. Nodal Lagrange and corresponding Edge polynomials constructed over 1D mesh with 4 GLL points.

If \mathcal{E} is a finite-dimensional vector space with n dimensions which has e_1, e_2, \dots, e_n as its basis, any arbitrary vector $v \in \mathcal{E}$ can be expanded as a linear combination of the basis vectors; $v = \sum_j v^j e_j$. Subsequently, applying the functional α to v yields:

$$\alpha(v) = \alpha\left(\sum_j v^j e_j\right) = \sum_j v^j \alpha(e_j). \tag{29}$$

Note that the linear functional α does *not* live in the vector space \mathcal{E} . Instead, the linear functional lives in a different space defined as follows.

Definition 3.2 ([28]). The collection of all the linear functionals on the vector space \mathcal{E} form a separate vector space referred to as the *dual space* denoted by \mathcal{E}^* . If \mathcal{E} is n -dimensional, then so is \mathcal{E}^* , which enables one to define the *dual basis* $\sigma^1, \sigma^2, \dots, \sigma^n$. The elements in the dual space are referred to as *covectors*. Furthermore, the canonical dual basis satisfies the property:

$$\sigma^i(e_j) = \delta_j^i, \tag{30}$$

which, along with the linearity of the σ^i , can be used to show that applying σ^i to a vector $v \in \mathcal{E}$ simply extracts the i th component of v

$$\sigma^i\left(\sum_j e_j v^j\right) = \sum_j \sigma^i(e_j) v^j = \sum_j \delta_j^i v^j = v^i. \tag{31}$$

The above definition can be used to construct a discrete dual space based on the primal spaces of Section 3.1. For the MSEM, the L^2 inner product was used to create such a space [26], which will be briefly explained in the next section.

3.3. L^2 dual basis

To construct the dual bases, we represent p^h with respect to a nodal basis as

$$p^h(\xi) = \sum_{i=0}^p \mathcal{N}_i^0(p^h) \psi_i^{(0)}(\xi). \tag{32}$$

In this equation, $\mathcal{N}_i^0(p^h)$ are the nodal degrees of freedom, and $\psi_i^{(0)}(\xi)$ are the associated basis functions (see (24)). For clarity, the following shorthand notation will be used [26],

$$p^h(\xi) = \boldsymbol{\psi}^{(0)}(\xi) \mathcal{N}^0(p^h), \tag{33}$$

where

$$\boldsymbol{\psi}^{(0)}(\xi) = \left[\psi_0^{(0)}(\xi) \quad \psi_1^{(0)}(\xi) \quad \dots \quad \psi_{p-1}^{(0)}(\xi) \quad \psi_p^{(0)}(\xi) \right] \quad \text{and} \quad \mathcal{N}^0(p^h) = \begin{bmatrix} \mathcal{N}_0^0(p^h) \\ \mathcal{N}_1^0(p^h) \\ \vdots \\ \mathcal{N}_{p-1}^0(p^h) \\ \mathcal{N}_p^0(p^h) \end{bmatrix}. \tag{34}$$

Now, let p^h and q^h be expanded as in (33). The L^2 -inner product between the two is then given by

$$(p^h, q^h)_{L^2(K)} = \int_K p^h(\xi)q^h(\xi) dK = \mathcal{N}^0(p^h)^T \mathbb{M}^{(0)} \mathcal{N}^0(q^h), \quad (35)$$

where $\mathbb{M}^{(0)}$ denotes the mass matrix built using the nodal basis functions as

$$\mathbb{M}^{(0)} = \int_K \boldsymbol{\psi}^{(0)}(\xi)^T \boldsymbol{\psi}^{(0)}(\xi) dK. \quad (36)$$

This mass matrix, and its inverse, can be used to define the dual degrees of freedom and the associated dual basis. The dual edge degrees of freedom (dual to the primal nodes) are then defined as

$$\widetilde{\mathcal{N}}^1(p^h) = \mathbb{M}^{(0)} \mathcal{N}^0(p^h). \quad (37)$$

Note that these are the degrees of freedom for the dual line elements. The dual basis functions are then

$$\widetilde{\boldsymbol{\psi}}^{(1)}(\xi) = \boldsymbol{\psi}^{(0)}(\xi) \mathbb{M}^{(0)-1}. \quad (38)$$

See [26] for the details and proofs. The plots of these dual edge polynomials are shown in Fig. 2(a).

Similarly, the basis dual to the primal edge polynomials can also be constructed. Defining p^h and q^h as

$$p^h(\xi) = \boldsymbol{\psi}^{(1)}(\xi) \mathcal{N}^1(p^h), \quad q^h(\xi) = \boldsymbol{\psi}^{(1)}(\xi) \mathcal{N}^1(q^h) \quad (39)$$

with

$$\boldsymbol{\psi}^{(1)}(\xi) = \left[\psi_1^{(1)}(\xi) \quad \psi_2^{(1)}(\xi) \quad \cdots \quad \psi_{p-1}^{(1)}(\xi) \quad \psi_p^{(1)}(\xi) \right] \quad \text{and} \quad \mathcal{N}^1(p^h) = \begin{bmatrix} \mathcal{N}_1^1(p^h) \\ \mathcal{N}_2^1(p^h) \\ \vdots \\ \mathcal{N}_{p-1}^1(p^h) \\ \mathcal{N}_p^1(p^h) \end{bmatrix}. \quad (40)$$

The L^2 -inner product is now given by

$$(p^h, q^h)_{L^2(K)} = \int_K p^h(\xi)q^h(\xi) dK = \mathcal{N}^1(p^h)^T \mathbb{M}^1 \mathcal{N}^1(q^h), \quad (41)$$

where $\mathbb{M}^{(1)}$ denotes the mass matrix built using the edge basis functions as

$$\mathbb{M}^{(1)} = \int_K \boldsymbol{\psi}^{(1)}(\xi)^T \boldsymbol{\psi}^{(1)}(\xi) dK. \quad (42)$$

Constructing the dual degrees of freedom and dual basis follows the exact same procedure as in the nodal case. Thus, the dual nodal degrees of freedom (dual to the primal edges) are defined as

$$\widetilde{\mathcal{N}}^0(p^h) = \mathbb{M}^{(1)} \mathcal{N}^1(p^h). \quad (43)$$

Note that these are the degrees of freedom for the dual nodal elements. The dual basis functions are then

$$\widetilde{\boldsymbol{\psi}}^{(0)}(\xi) = \boldsymbol{\psi}^{(1)}(\xi) \mathbb{M}^{(1)-1}. \quad (44)$$

See again [26] for the details and proofs. The plots of these dual polynomials are shown in Fig. 2(b).

The primal and dual bases discussed thus far have all been defined in a single (reference) domain $\xi \in K = [-1, 1]$. For the generalisation to a multi-element setting over an arbitrary physical domain $x \in \Omega = [a, b]$ divided into N elements with $a, b \in \mathbb{R}$ and $a = x_0 < x_1 < \cdots < x_{N-1} < x_N = b$, we introduce the following linear map Φ between K and $[x_{n-1}, x_n]$

$$x = \Phi(\xi) = \frac{1}{2}(1 - \xi)x_{n-1} + \frac{1}{2}(1 + \xi)x_n, \quad -1 \leq \xi \leq 1. \quad (45)$$

Subsequently, the global nodal basis functions are defined as

$$\boldsymbol{\psi}_i^{(0)}(x) = \boldsymbol{\psi}_j^{(0)}(\xi) \circ \Phi^{-1}(x) \quad \text{with } i = j + (n-1)p, \quad (46)$$

where $n = 1, \dots, N$ and $j = 0, \dots, p$, giving a total of $k = p + 1 + (N-1)p$ nodal functions. Similarly, the global edge basis functions are given by

$$\boldsymbol{\psi}_i^{(1)}(x) = \boldsymbol{\psi}_j^{(1)}(\xi) \circ \frac{\Phi^{-1}(x)}{\mathbf{J}} \quad \text{with } i = j + (n-1)p, \quad (47)$$

where $n = 1, \dots, N$ and $j = 1, \dots, p$, and $\mathbf{J} = \frac{dx}{d\xi}$ is the Jacobian, giving a total of $k = p + (N-1)p$ edge functions. Further details regarding the multi-element case may be found in [26, Section 2.3].

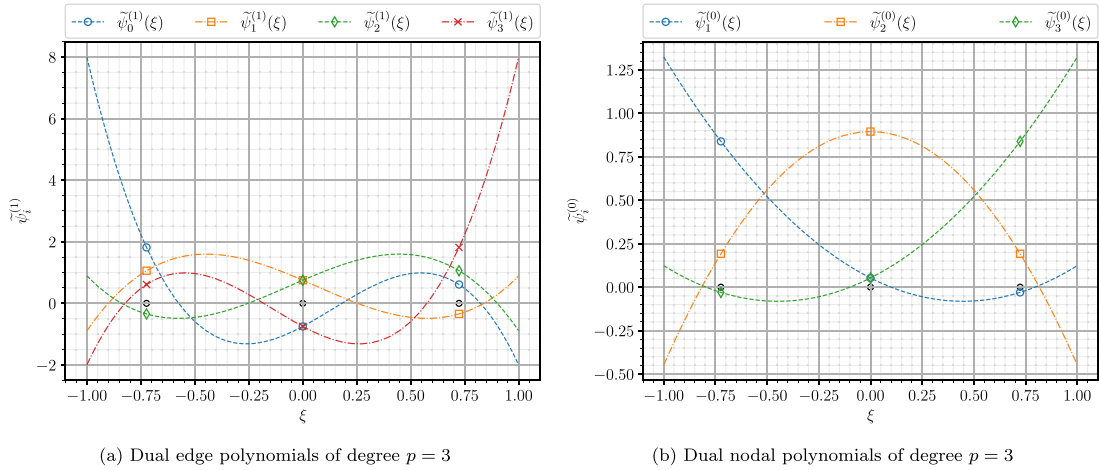


Fig. 2. Dual nodal and edge polynomials constructed over 1D mesh with 4 GLL points.

3.4. Projections

We define the projections as follows

Definition 3.3. Consider a real-valued infinite-dimensional function space V and a finite-dimensional function subspace \bar{V} . A *projection* is the mapping $\mathcal{P} : V \rightarrow \bar{V}$ from the infinite-dimensional space to the finite-dimensional one which minimises the difference between the infinite and finite-dimensional representations in a given norm.

3.4.1. L^2 projection

Effectively, the projection maps continuous quantities (functions) into the discrete finite-dimensional subspace such that the best possible discrete representation in the considered norm is obtained. We will show that dual basis functions encode the projector. To demonstrate this fact, consider the L^2 projection \mathcal{P}_{L^2} of a function $\phi \in L^2(\Omega)$. The minimisation problem thus reads

$$\mathcal{P}_{L^2} \phi = \arg \min_{\bar{\phi} \in \bar{V}} \left\{ \frac{1}{2} \|\bar{\phi} - \phi\|_{L^2}^2 \right\}, \tag{48}$$

which gives

$$(v^h, \bar{\phi})_{L^2(\Omega)} = (v^h, \phi)_{L^2(\Omega)}, \quad \forall v^h \in \bar{V}. \tag{49}$$

Considering a 1D case and expanding $\bar{\phi}$ in terms of primal edge polynomials and v_h in terms of the corresponding dual basis given by (43) and (44)

$$\bar{\phi} := \psi^{(1)} \mathcal{N}^1(\bar{\phi}) \tag{50}$$

$$v^h := \tilde{\psi}^{(0)} \tilde{\mathcal{N}}^0(v^h), \tag{51}$$

we obtain after substitution of these expansions into (49),

$$\tilde{\mathcal{N}}^0(v^h)^T \left(\tilde{\psi}^{(0)}, \psi^{(1)} \right)_{L^2(\Omega)} \mathcal{N}^1(\bar{\phi}) = \tilde{\mathcal{N}}^0(v^h)^T \left(\tilde{\psi}^{(0)}, \phi \right)_{L^2(\Omega)}, \quad \forall \tilde{\mathcal{N}}^0(v^h) \in \mathbb{R}^k. \tag{52}$$

Using the fact that the primal and the dual bases are bi-orthogonal, i.e. $\left(\tilde{\psi}_i^{(0)}, \psi_j^{(1)} \right)_{L^2(\Omega)} = \delta_{i,j}$, we have

$$\mathcal{N}^1(\bar{\phi}) = \left(\mu^{L^2}, \phi \right)_{L^2(\Omega)}, \tag{53}$$

where we introduced $\mu^{L^2} = \tilde{\psi}^{(0)}$. This indicates that the inner product between the L^2 dual basis and any $\phi \in L^2(\Omega)$ returns the expansion coefficients for the projection of ϕ onto \bar{V} . The projected solution is then obtained using the primal edge functions, (50). The plots of these L^2 dual functions in a multi-element setting are shown in Figs. 3 and 4 for different polynomial degrees.

Remark 3.2. We choose the space of edge basis functions to expand the functions in \bar{V} for the L^2 projection for the reason that the edge functions live strictly in the L^2 space. We may, however, also choose to expand $\bar{\phi}$ in nodal basis functions which would give us the nodal L^2 projection.

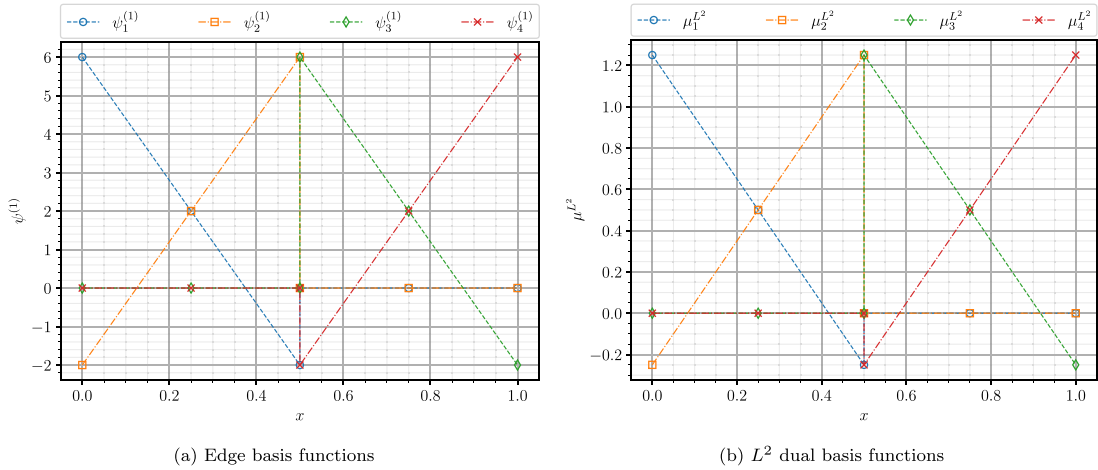


Fig. 3. Primal edge basis functions of polynomial degree $p = 2$ over 2 elements and their corresponding L^2 duals over $x \in \Omega \in [0, 1]$.

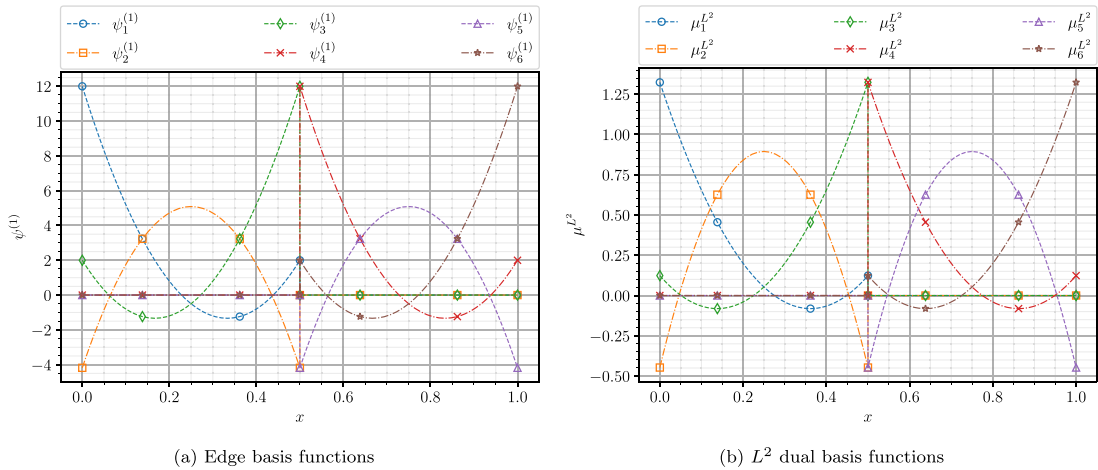


Fig. 4. Primal edge basis functions of polynomial degree $p = 3$ over 2 elements and their corresponding L^2 duals over $x \in \Omega \in [0, 1]$.

3.4.2. H_0^1 Projection

The concept introduced need not be limited to L^2 . This may also be extended to other projections giving rise to different sets of dual basis functions. For instance, considering the H_0^1 projection yields the H_0^1 dual basis functions. We consider the H_0^1 projection in a manner similar to that for the L^2 but with the projector $\mathcal{P}_{H_0^1}$. For $\phi \in H_0^1(\Omega)$ the minimisation problem reads

$$\mathcal{P}_{H_0^1} \phi = \arg \min_{\bar{\phi} \in \bar{V}} \left\{ \frac{1}{2} \|\nabla \bar{\phi} - \nabla \phi\|_{L^2}^2 \right\}, \tag{54}$$

which leads to

$$(v^h, \bar{\phi})_{H_0^1(\Omega)} = (v^h, \phi)_{H_0^1(\Omega)}, \quad \forall v^h \in \bar{V}. \tag{55}$$

For the 1D case, we substitute

$$\bar{\phi} := \boldsymbol{\Psi}^{(0)} \mathcal{N}^0(\bar{\phi}) \tag{56}$$

$$-\Delta_h v^h := \boldsymbol{\Psi}^{(0)} \mathcal{N}^0(v^h) \iff v^h = (-\Delta_h^{-1} \boldsymbol{\Psi}^{(0)}) \mathcal{N}^0(v^h), \tag{57}$$

into (55) where Δ_h^{-1} is the discrete inverse Laplacian operator with homogeneous Dirichlet boundaries, and we get

$$\mathcal{N}^0(v^h)^T (-\Delta_h^{-1} \boldsymbol{\Psi}^{(0)}, \boldsymbol{\Psi}^{(0)})_{H_0^1(\Omega)} \mathcal{N}^0(\bar{\phi}) = \mathcal{N}^0(v^h)^T (-\Delta_h^{-1} \boldsymbol{\Psi}^{(0)}, \phi)_{H_0^1(\Omega)}, \quad \forall \mathcal{N}^0(v^h) \in \mathbb{R}^k. \tag{58}$$

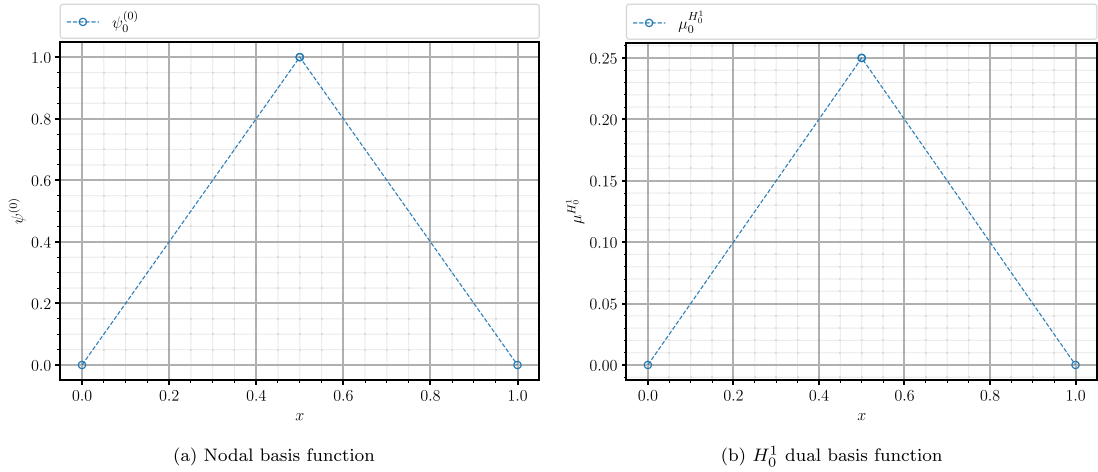


Fig. 5. Primal nodal basis function of polynomial degree $p = 1$ over 2 elements and its corresponding H_0^1 dual over $x \in \Omega \in [0, 1]$.

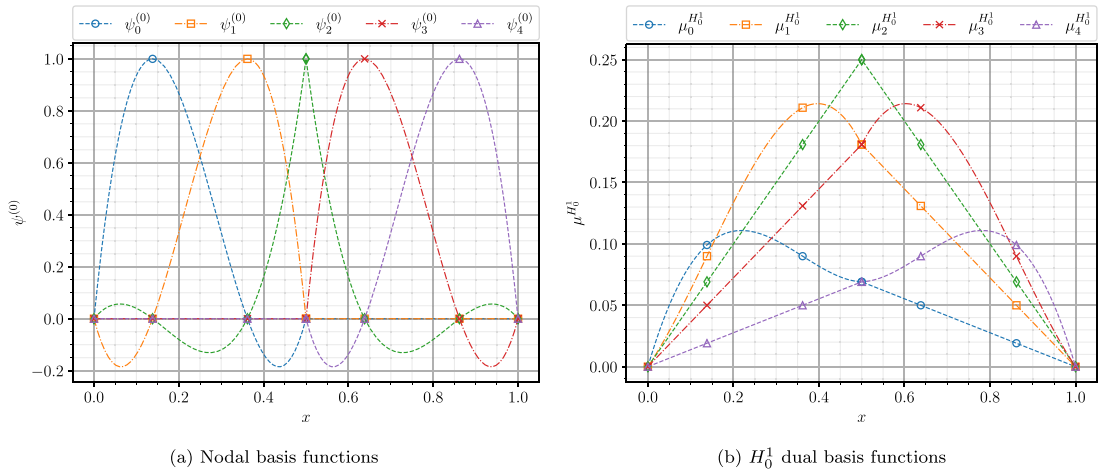


Fig. 6. Primal nodal basis functions of polynomial degree $p = 3$ over 2 elements and their corresponding H_0^1 duals over $x \in \Omega \in [0, 1]$.

Using the fact that $(-\Delta_h^{-1} \psi_i^{(0)}, \psi_j^{(0)})_{H_0^1(\Omega)} = \delta_{i,j}$ and the fact that this equation needs to hold for all $\mathcal{N}^0(v^h) \in \mathbb{R}^k$ gives

$$\mathcal{N}^0(\bar{\phi}) = (-\Delta_h^{-1} \psi^{(0)}, \phi)_{H_0^1(\Omega)}. \tag{59}$$

If we define $\mu^{H_0^1}$ to be the solution of $-\Delta_h \mu^{H_0^1} = \psi^{(0)}$, this can be written as

$$\mathcal{N}^0(\bar{\phi}) = (\mu^{H_0^1}, \phi)_{H_0^1(\Omega)}. \tag{60}$$

Once again, when the expansion coefficients $\mathcal{N}^0(\bar{\phi})$ are obtained from (60), and we use (56) to produce the H_0^1 projected solution in \bar{V} .

Remark 3.3. The functionals μ defined in Sections 3.4.1 and 3.4.2, are explicitly computable, and play the role of the $\{\mu_i\}_{i=1,\dots,N}$ described in the paper of Hughes and Sangalli, [25, (2.17)].

Plots of these dual bases are presented in Figs. 5 and 6. It is evident that the H_0^1 dual functions are all positive functions and inherently global.

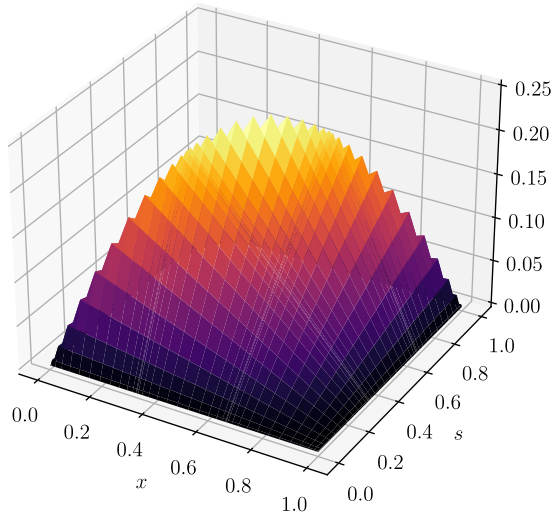


Fig. 7. Greens' function for the 1D Poisson in $\Omega = [0, 1]$.

4. Fine-scale Greens' function

Having reviewed the formulation of the Fine-Scale Greens' function and proposing to define the μ 's as dual basis functions, we now proceed to construct the Fine-Scale Greens' function. In this section, we present the various computations involved in constructing the Fine-Scale Greens' function for the 1D Poisson equation associated with both the H_0^1 and L^2 projections.

4.1. Computing the fine-scale Greens' function for 1D Poisson

The 1D Poisson problem is stated as follows

$$-\frac{\partial^2 u}{\partial x^2} = f, \quad x \in \Omega = [0, 1] \tag{61}$$

$$u(x) = 0, \quad x \in \partial\Omega. \tag{62}$$

The (global) Greens' function for this problem defined in Ω is given by

$$g(x, s) = \begin{cases} (1-s)x, & x \leq s \\ s(1-x), & x > s, \end{cases} \tag{63}$$

the plot of which is shown in Fig. 7.

Using the Greens' function and the μ defined by the dual basis, the Fine-Scale Greens' function from (22) may be computed componentwise. We start with the term $\mathcal{G}\mu^T$ which is a row vector defined as

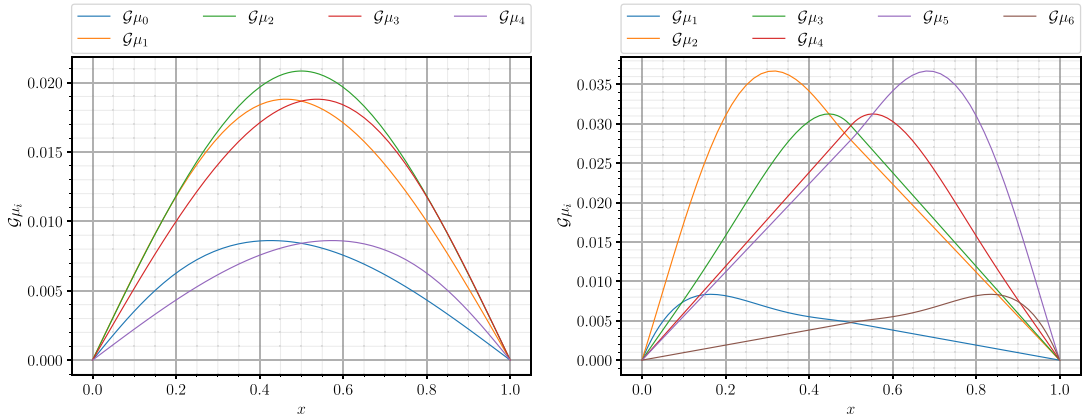
$$\mathcal{G}\mu^T = [\mathcal{G}\mu_0, \mathcal{G}\mu_1, \dots, \mathcal{G}\mu_k], \quad \text{with } \mathcal{G}\mu_i := \int_{\Omega} g(x, s)\mu_i(s) \, ds, \tag{64}$$

where the components of the vector correspond to the solution of the underlying PDE (the Poisson equation in this case) with μ as right hand side term. Similarly, the matrix $\mu\mathcal{G}\mu^T$ is computed as follows

$$\mu\mathcal{G}\mu^T = \begin{bmatrix} v^* \langle \mu_0, \mathcal{G}\mu_0 \rangle_V & \dots & v^* \langle \mu_0, \mathcal{G}\mu_k \rangle_V \\ \vdots & \ddots & \vdots \\ v^* \langle \mu_k, \mathcal{G}\mu_0 \rangle_V & \dots & v^* \langle \mu_k, \mathcal{G}\mu_k \rangle_V \end{bmatrix}, \tag{65}$$

where the columns can be recognised as the projection of $\mathcal{G}\mu^T$ onto \bar{V} . As such, we have to respect that the entries of the matrix are duality pairings, meaning that for the H_0^1 projection, we have:

$$\mu\mathcal{G}\mu^T = \begin{bmatrix} (\mu_0, \mathcal{G}\mu_0)_{H_0^1(\Omega)} & \dots & (\mu_0, \mathcal{G}\mu_k)_{H_0^1(\Omega)} \\ \vdots & \ddots & \vdots \\ (\mu_k, \mathcal{G}\mu_0)_{H_0^1(\Omega)} & \dots & (\mu_k, \mathcal{G}\mu_k)_{H_0^1(\Omega)} \end{bmatrix}, \quad \text{with } (\mu_i, \mathcal{G}\mu_j)_{H_0^1(\Omega)} := \int_{\Omega} \frac{\partial \mu_i}{\partial x} \frac{\partial \mathcal{G}\mu_j}{\partial x} \, dx, \tag{66}$$



(a) \mathcal{G}_{μ_i} with H_0^1 dual basis functions from Figure 6 as source term (b) \mathcal{G}_{μ_i} with L^2 dual basis functions from Figure 4 as source term

Fig. 8. \mathcal{G}_{μ_i} computed with H_0^1 and L^2 dual basis functions for the Poisson equation.

and similarly for the L^2 projection we have:

$$\boldsymbol{\mu} \mathcal{G} \boldsymbol{\mu}^T = \begin{bmatrix} (\mu_0, \mathcal{G}\mu_0)_{L^2(\Omega)} & \cdots & (\mu_0, \mathcal{G}\mu_k)_{L^2(\Omega)} \\ \vdots & \ddots & \vdots \\ (\mu_k, \mathcal{G}\mu_0)_{L^2(\Omega)} & \cdots & (\mu_k, \mathcal{G}\mu_k)_{L^2(\Omega)} \end{bmatrix}, \quad \text{with } (\mu_i, \mathcal{G}\mu_j)_{L^2(\Omega)} := \int_{\Omega} \mu_i \mathcal{G}\mu_j \, dx. \tag{67}$$

The components of $\mathcal{G}\boldsymbol{\mu}^T$ are plotted in Fig. 8 for both the H_0^1 and L^2 projections. $\boldsymbol{\mu} \mathcal{G} \boldsymbol{\mu}^T$ is then found by using (65) with the computed $\mathcal{G}\boldsymbol{\mu}^T$.

Lastly, we consider the term $\boldsymbol{\mu} \mathcal{G}$ which is a functional expressed as a column vector defined as

$$\boldsymbol{\mu} \mathcal{G}(v) = \begin{bmatrix} v^* \langle \mu_0, \mathcal{G}v \rangle_V \\ \vdots \\ v^* \langle \mu_k, \mathcal{G}v \rangle_V \end{bmatrix}, \quad \forall v \in V^*. \tag{68}$$

The act of applying $\boldsymbol{\mu} \mathcal{G}$ to an arbitrary function $v \in V^*$ is equivalent to computing the projection of the solution to the underlying PDE with v as its source term. Computing the components of $\boldsymbol{\mu} \mathcal{G}$ is rather complicated, specifically for the H_0^1 projection. In particular, the issue arises from the duality pairing which requires the derivative of the piece-wise smooth Greens' function

$$(\mu_i, \mathcal{G}v)_{H_0^1(\Omega)} = \left[\int_{\Omega} \frac{\partial \mu_i}{\partial x} \frac{\partial \mathcal{G}}{\partial x} \, dx \right] v. \tag{69}$$

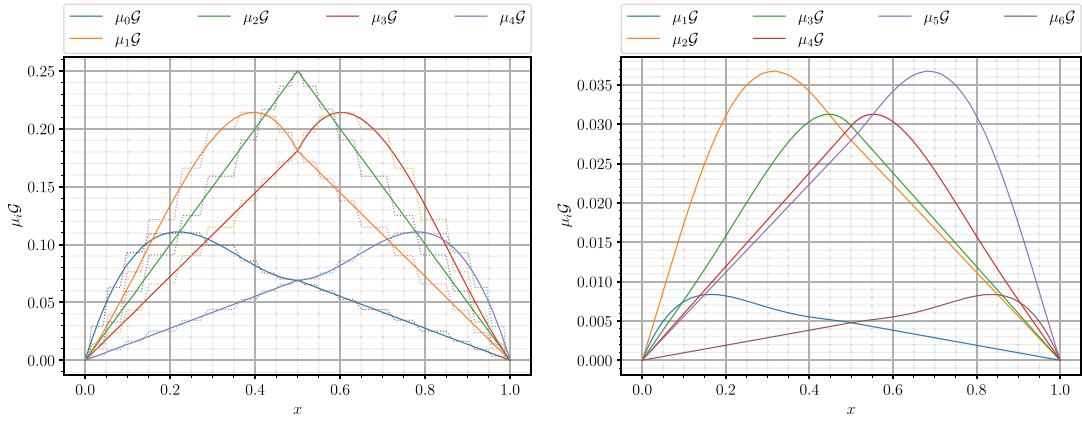
Attempting to compute these integrals using standard quadrature rules will yield very poor results stemming from the fact that the discontinuity in $\frac{\partial \mathcal{G}}{\partial x}$ will not be adequately captured by the quadrature. To resolve this issue, we split up the integral over the domain based on the known location of the discontinuity of $\frac{\partial \mathcal{G}}{\partial x}$ (along $x = s$) and use the standard Gauss Lobatto quadrature to integrate the smooth functions on either side of the discontinuity. In contrast, for the L^2 case, $\boldsymbol{\mu} \mathcal{G}$ may be computed directly with standard quadrature as it only involves the L^2 pairing between $\boldsymbol{\mu}$ and \mathcal{G} . Plots for the components of $\boldsymbol{\mu} \mathcal{G}$ computed using the dual basis functions from Figs. 4 and 6 are shown in Fig. 9. Moreover, Fig. 9(a) shows $\boldsymbol{\mu} \mathcal{G}$ computed using two separate methods, where the solid lines correspond to the aforementioned discontinuity splitting integral approach and the dotted lines corresponding to the standard quadrature rule.

In the specific case of the Poisson equation and the H_0^1 projection, the entries of $\boldsymbol{\mu} \mathcal{G}$ simply yield the μ 's themselves as is apparent in Fig. 9(a). This is attributed to the fact that the H_0^1 projection encodes the Poisson problem as the projector is the differential operator. Consider u_{exact} to be the exact (strong) solution to (61) satisfying (62), from (60) we note that the H_0^1 projection (\bar{u}) of u_{exact} is given by

$$\mathcal{N}^0(\bar{u}) = \left(\boldsymbol{\mu}^{H_0^1}, u_{exact} \right)_{H_0^1(\Omega)} \rightarrow \bar{u} = \boldsymbol{\psi}^{(0)} \mathcal{N}^0(\bar{u}). \tag{70}$$

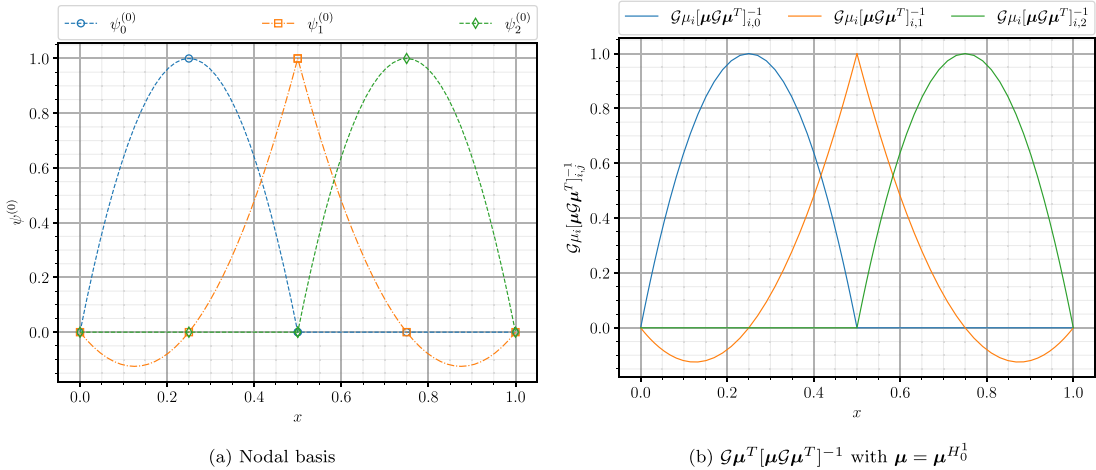
Applying the pairing and employing integration by parts yields

$$\mathcal{N}^0(\bar{u}) = \int_{\Omega} \frac{\partial \boldsymbol{\mu}^{H_0^1}}{\partial x} \frac{\partial u_{exact}}{\partial x} \, dx = \cancel{\boldsymbol{\mu}^{H_0^1} \frac{\partial u_{exact}}{\partial x} \Big|_{\partial \Omega}} - \int_{\Omega} \boldsymbol{\mu}^{H_0^1} \frac{\partial^2 u_{exact}}{\partial x^2} \, dx, \tag{71}$$



(a) $\mu_i \mathcal{G}$ computed using the H_0^1 dual basis functions from Figure 6 (b) $\mu_i \mathcal{G}$ computed using the L^2 dual basis functions from Figure 4

Fig. 9. $\mu_i \mathcal{G}$ computed with H_0^1 and L^2 dual basis functions for the Poisson equation with the solid and dotted lines in Fig. 9(a) corresponding to the discontinuity splitting integral approach and the standard quadrature rule, respectively.



(a) Nodal basis

(b) $\mathcal{G} \mu_i [\mu \mathcal{G} \mu^T]^{-1}$ with $\mu = \mu^{H_0^1}$

Fig. 10. Mesh with polynomial degree $p = 2$ and 2 elements.

where the boundary term emerging from the integration by parts vanishes due to $\mu^{H_0^1}$ being zero at the boundaries. Moreover, since u_{exact} satisfies (61), we have

$$\mathcal{N}^0(\bar{u}) = \int_{\Omega} \mu^{H_0^1} f \, dx, \tag{72}$$

by which is it evident that the Poisson problem is embedded in the H_0^1 projection. It further implies that the exact H_0^1 projection of the Poisson equation can be computed without ever requiring the exact solution.

With all these components in place, the Fine-Scale Greens' function may be assembled. Before doing so, however, it is worthwhile reviewing the sequence of mappings associated with the Fine-Scale Greens' function. The full expression for computing u' reads

$$u' = \mathcal{G} \mathcal{R} \bar{u} - \mathcal{G} \mu^T [\mu \mathcal{G} \mu^T]^{-1} \mu \mathcal{G} \mathcal{R} \bar{u}, \tag{73}$$

where we see the first term ($\mathcal{G} \mathcal{R} \bar{u}$) is the (global) Greens' function applied to the residual of the resolved scales. The same term appears in the second term of (73), but there it is accompanied by μ , which indicates it is being projected onto the finite-dimensional resolved space. The remaining component $\mathcal{G} \mu^T [\mu \mathcal{G} \mu^T]^{-1}$ is rather interesting as it reproduces the resolved scale basis as shown in Figs. 10 and 11.

The term $\mathcal{G} \mu^T [\mu \mathcal{G} \mu^T]^{-1}$ can thus be seen as a reconstruction/interpolation operator mapping discrete quantities from the resolved finite-dimensional space to the continuous space. Therefore, the term $\mathcal{G} \mu^T [\mu \mathcal{G} \mu^T]^{-1} \mu \mathcal{G} \mathcal{R} \bar{u}$ simply equates to the component of $\mathcal{G} \mathcal{R} \bar{u}$ that lives in the resolved space. Note, it is not a projection of the residual, but rather the projection of \mathcal{G} applied to the residual.

Figs. 12(a) and 12(b) show the resulting Fine-Scale Greens' functions for the H_0^1 and L^2 projections, respectively. Furthermore, Figs. 13 and 14 show the H_0^1 Fine-Scale Greens' function alongside the localised Element's Greens' function for $p = 1$ and $p = 2$.

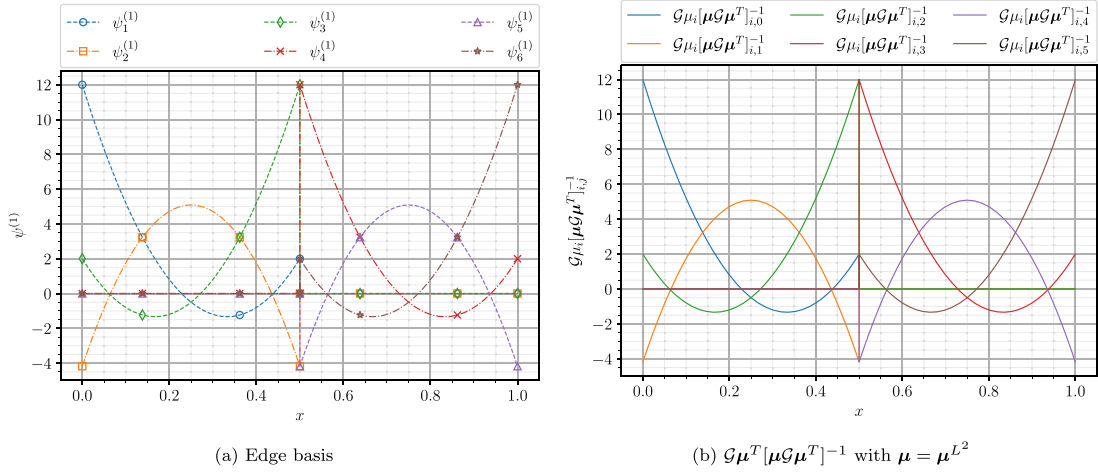


Fig. 11. Mesh with polynomial degree $p = 3$ and 2 elements.

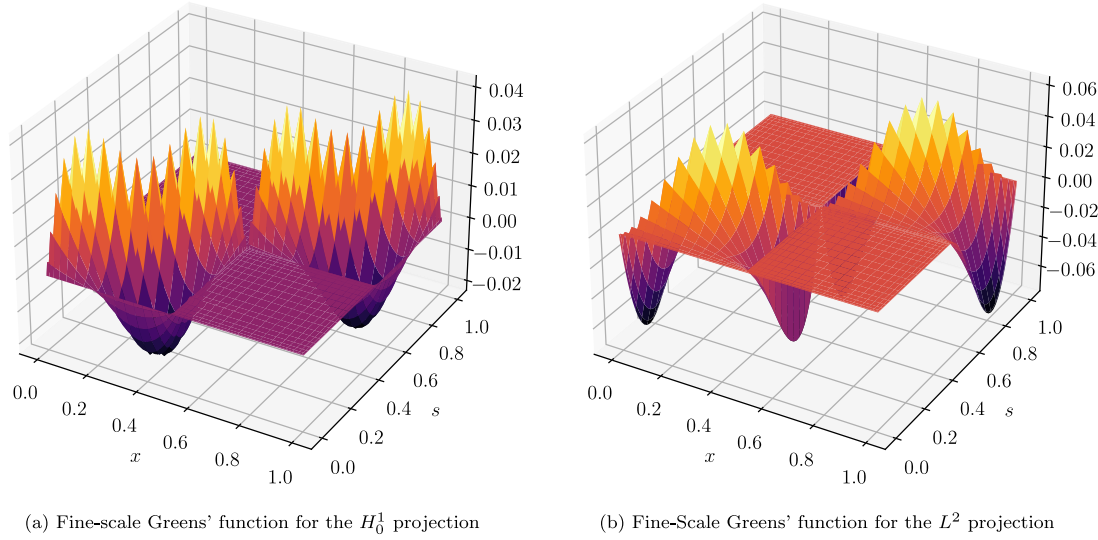


Fig. 12. Fine-Scale Greens' functions for 1D Poisson equation on a mesh with polynomial degree $p = 2$ and 2 elements.

Here we find that the Fine-Scale Greens' function for the $p = 1$ case exactly corresponds to the local Element's Greens' function. This, however, is no longer true for $p > 1$.

4.2. Reconstruction of fine-scale terms of a projection for 1D Poisson

In order to carry out numerical tests with the constructed Fine-Scales Greens' function, we consider the sample Poisson problem from (61) with

$$f = 4\pi^2 \sin(2\pi x), \tag{74}$$

for which the exact solution is given by

$$u_{exact} = \sin(2\pi x). \tag{75}$$

We then compute the exact H_0^1 and L^2 projections of the exact solution using the corresponding dual basis functions as previously described. The plots of the exact solution along with its H_0^1 and L^2 projections onto the finite-dimensional mesh are shown in Figs. 15(a) and 16(a) for two polynomial approximations. Once again, we choose a L^2 projection that maps onto the space of edge polynomials following the line of reasoning in Remark 3.2. As a consequence, the degree of polynomials spanning the L^2 space is $(p - 1)$ (see Remark 3.1).

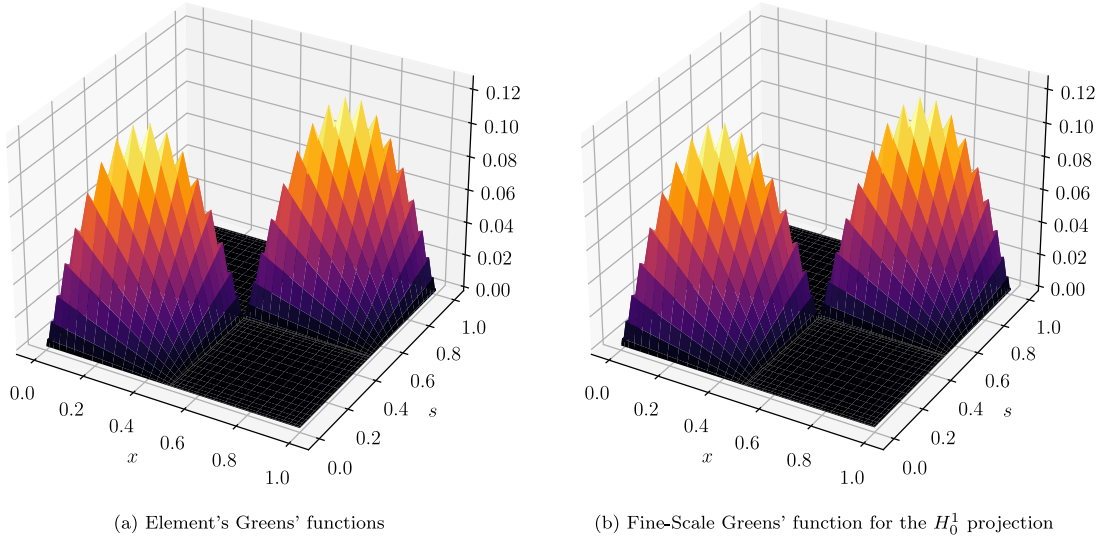


Fig. 13. Greens' functions for 1D Poisson equation on a mesh with polynomial degree $p = 1$ and 2 elements.

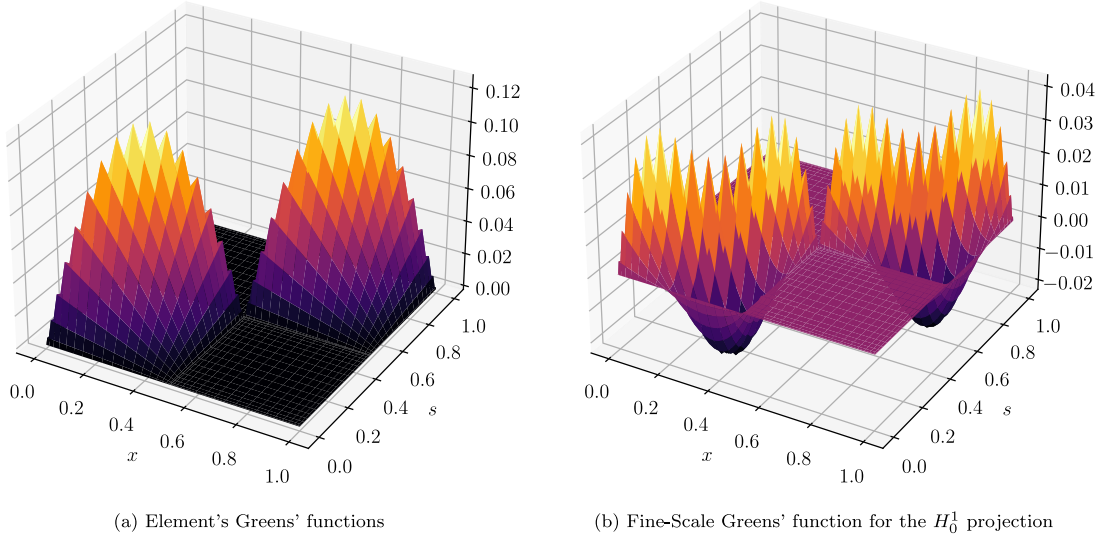


Fig. 14. Greens' functions for 1D Poisson equation on a mesh with polynomial degree $p = 2$ and 2 elements.

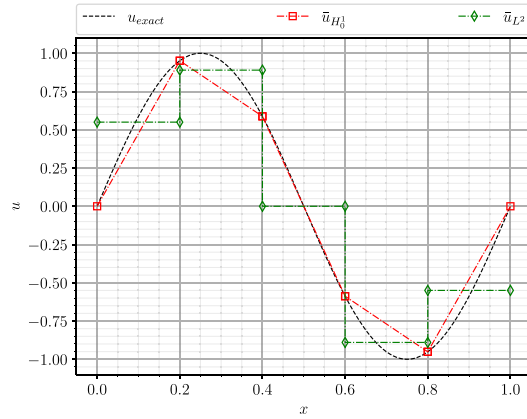
Applying the respective Fine-Scale Greens' functions to the residual of the respective projections yields the exact unresolved scales of the projections as shown in Figs. 15(b) and 16(b) for the H_0^1 projection and Figs. 15(c) and 16(c) for the L^2 projection. These figures also include the plots of the individual components $\mathcal{G}\mathcal{R}\bar{u}$ and $\mathcal{G}\mu^T [\mu\mathcal{G}\mu^T]^{-1} \mu\mathcal{G}\mathcal{R}\bar{u}$. These individual components highlight the main characteristic of the Fine-Scale Greens' function, namely the subtraction of the component of $\mathcal{G}\mathcal{R}\bar{u}$ that lives in the resolved space.

4.3. Computing the fine-scale terms of a projection for 1D advection–diffusion

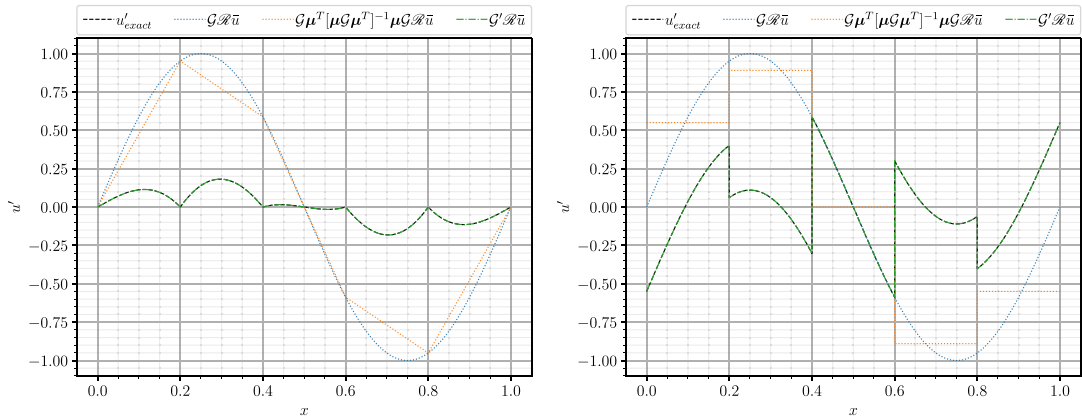
In a manner similar to that considered for the 1D Poisson equation, we can apply this approach to construct the Fine-Scale Greens' function for the 1D advection–diffusion equation. The governing equation for the 1D advection–diffusion problem reads as follows

$$c \frac{\partial u}{\partial x} - v \frac{\partial^2 u}{\partial x^2} = f, \quad x \in \Omega = [0, 1] \tag{76}$$

$$u(x) = 0, \quad x \in \partial\Omega, \tag{77}$$



(a) Exact solution to sample Poisson equation and its H_0^1 and L^2 projections



(b) Fine scales for H_0^1 projection computed using the Fine-Scale Greens' functions (c) Fine scales for L^2 projection computed using the Fine-Scale Greens' functions

Fig. 15. Mesh with polynomial degree $p = 1$ and 5 elements.

with the constants, c and ν being the advection speed and diffusion coefficient, respectively.

In this simple 1D setting, the global Greens' function for the advection–diffusion equation in Ω can be found to be

$$g(x, s) = \begin{cases} \frac{1 - e^{-2\alpha(1 - \frac{x}{h})}}{c(1 - e^{-2\alpha})} \left(1 - e^{-2\alpha \frac{s}{h}} \right), & x \leq s \\ \frac{e^{2\alpha \frac{x}{h}} - 1}{c(1 - e^{-2\alpha})} \left(e^{-2\alpha \frac{s}{h}} - e^{-2\alpha} \right), & x > s \end{cases} \tag{78}$$

$$\alpha = \frac{ch}{2\nu}, \tag{79}$$

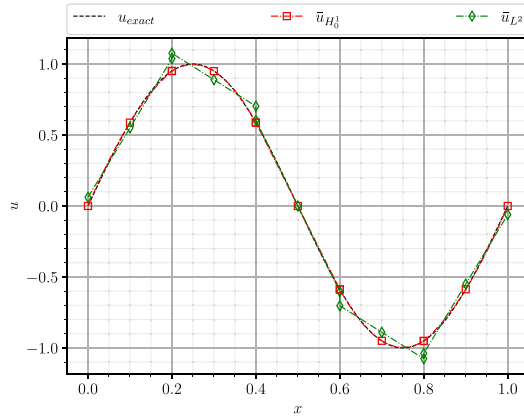
where h is the domain width and α is the mesh Peclet number. In theory, we can take this Greens' function and construct the Fine-Scale Greens' function for any projector using the aforementioned approach. This poses two notable complications, however, one relating to the integration of the Greens' function's sharp gradients at high Peclet numbers and the second being the loss of generality in multi-dimensional settings where the global Greens' function of the advection–diffusion problem is not readily available. We therefore adopt an alternate approach for the advection–diffusion problem which bypasses these shortcomings.

This entails rewriting the advection–diffusion equation as a Poisson problem with a modified right hand side term as follows

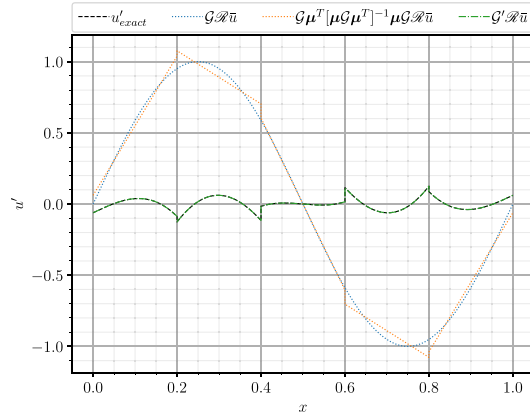
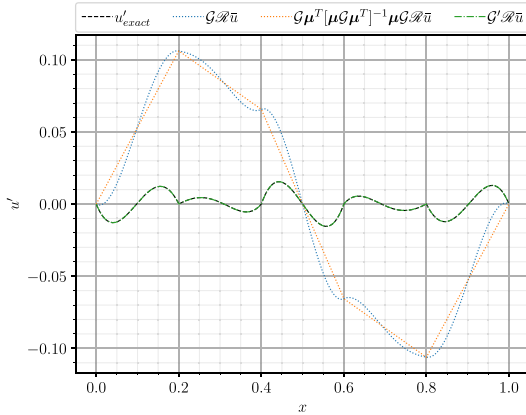
$$-\frac{\partial^2 u}{\partial x^2} = \frac{1}{\nu} f - \frac{c}{\nu} \frac{\partial u}{\partial x}, \tag{80}$$

for which the resolved component of the variational form reads

$$-\frac{1}{\nu^*} \left\langle \frac{\partial^2 \bar{u}}{\partial x^2}, \bar{v} \right\rangle_V - \frac{1}{\nu^*} \left\langle \frac{\partial^2 u'}{\partial x^2}, \bar{v} \right\rangle_V = \frac{1}{\nu^*} \left\langle \left(\frac{1}{\nu} f - \frac{c}{\nu} \frac{\partial u}{\partial x} \right), \bar{v} \right\rangle_V \quad \forall \bar{v} \in \bar{V}, \tag{81}$$



(a) Exact solution to sample Poisson equation and its H_0^1 and L^2 projections



(b) Fine scales for H_0^1 projection computed using the Fine-Scale Greens' functions

(c) Fine scales for L^2 projection computed using the Fine-Scale Greens' functions

Fig. 16. Mesh with polynomial degree $p = 2$ and 5 elements.

and the fine scales may be computed using the Fine-Scale Greens' function for Poisson equation as follows

$$u' = \mathcal{G}' \mathcal{R} \bar{u} = \mathcal{G}' \left(\left(\frac{1}{v} f - \frac{c}{v} \frac{\partial u}{\partial x} \right) + \frac{\partial^2 \bar{u}}{\partial x^2} \right). \tag{82}$$

Note that in the diffusive limit with $c = 0$ this reverts back to the formulation for the Poisson equation. Another important thing to note is that the advection term $\frac{\partial u}{\partial x}$ appearing in the residual is the gradient of the exact solution and not \bar{u} . This term thus needs special treatment which will be discussed shortly. We will first demonstrate how this formulation reconstructs the fine scales for the projections in Section 4.4, when we substitute the known exact derivative of the solution in the residual. Thereafter in Section 4.5, we describe an iterative approach which overcomes the need to have the exact derivative of the solution.

4.4. Reconstruction of fine-scale terms of a projection for 1D advection–diffusion

We consider the advection–diffusion equation from (76) with the following input parameters

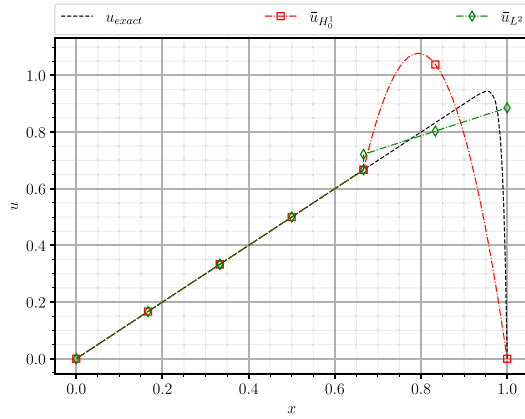
$$f = 1, \quad c = 1, \quad v = 0.01, \quad \alpha = 50 \tag{83}$$

for which the exact solution and the exact solution gradient are given by

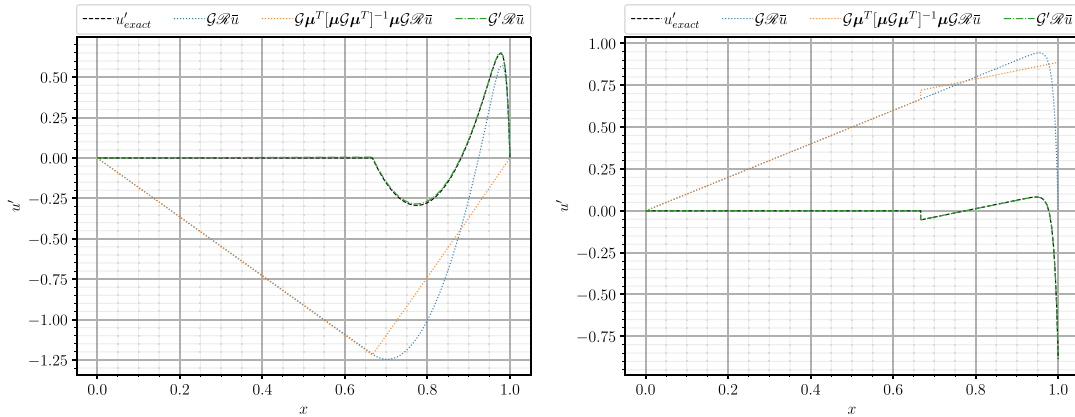
$$u_{exact} = \frac{1}{c} \left(x - \frac{e^{\alpha(x-1)} - e^{-\alpha}}{1 - e^{-\alpha}} \right) \tag{84}$$

$$\frac{\partial u_{exact}}{\partial x} = \frac{1}{c} \left(1 - \frac{\alpha e^{\alpha(x-1)}}{1 - e^{-\alpha}} \right) \tag{85}$$

The plot of the exact solution and its H_0^1 and L^2 projections onto different meshes are shown in Figs. 17(a) and 18(a). The exact fine scales and the reconstruction thereof using the (Poisson) Fine-Scale Greens' function are shown in Figs. 17(b) and 18(b) for the



(a) Exact solution to advection-diffusion equation and its H_0^1 and L^2 projections with $\alpha = 50$



(b) Fine-scales for H_0^1 projection computed using the Fine-Scale Greens' functions (c) Fine-scales for L^2 projection computed using the Fine-Scale Greens' functions

Fig. 17. Mesh with polynomial degree $p = 2$ and 3 elements.

H_0^1 projection and in Figs. 17(c) and 18(c) for the L^2 projection. As evident from these figures, the proposed formulation correctly reconstructs all the fine scales missing in the projection. However, as noted before, this approach required the gradient of the exact solution to be available which makes it unusable for any VMS formulation in practice.

4.5. Iterative VMS approach

The need for the derivative of the exact solution in the above demonstration can be avoided using an iterative procedure. The goal of this iterative approach is to produce a VMS formulation for the advection–diffusion equation which yields the exact projection and the missing fine scales. Here, we focus on the H_0^1 projection, motivated by the fact that the exact solution lives in the H_0^1 space. We note, however, that this iterative concept is not limited to H_0^1 and can be extended to other projections.

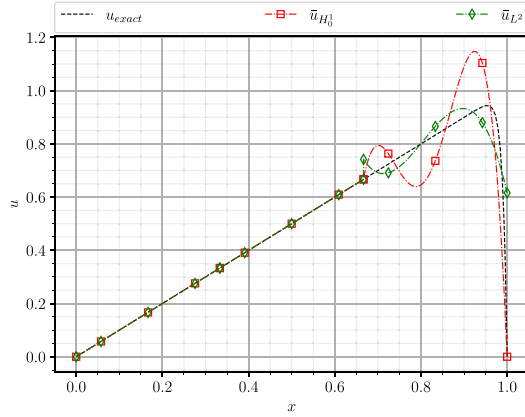
To construct an iterative approach that solves for H_0^1 projection, we start with the resolved scale equation from (81) where we take $v = \mu^{H_0^1}$ as the test functions and apply an L^2 pairing

$$-\left(\mu^{H_0^1}, \frac{\partial^2 u}{\partial x^2}\right)_{L^2(\Omega)} = \left(\mu^{H_0^1}, \frac{1}{v} f\right)_{L^2(\Omega)} - \left(\mu^{H_0^1}, \frac{c}{v} \frac{\partial u}{\partial x}\right)_{L^2(\Omega)}. \tag{86}$$

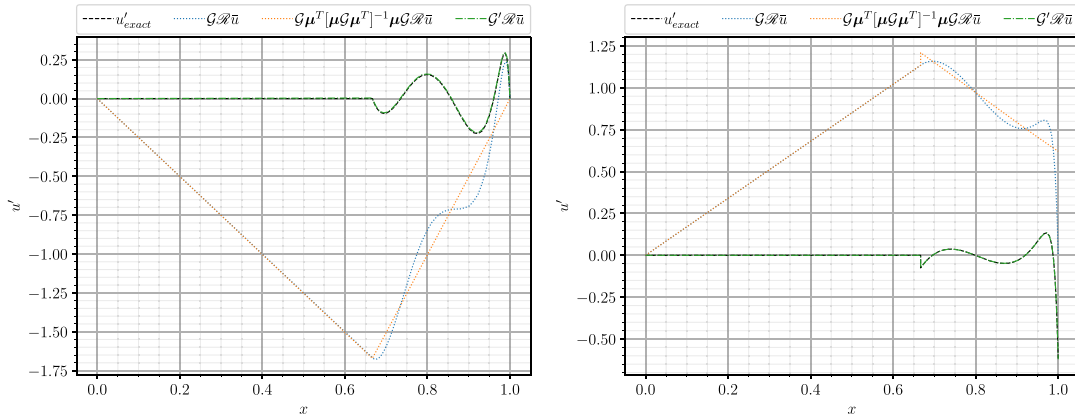
If we apply integration by parts to the left-hand side, we get

$$-\cancel{\mu^{H_0^1} \frac{\partial u}{\partial x}} \Big|_{\partial\Omega} + \left(\frac{\partial \mu^{H_0^1}}{\partial x}, \frac{\partial u}{\partial x}\right)_{L^2(\Omega)} = \left(\mu^{H_0^1}, \frac{1}{v} f\right)_{L^2(\Omega)} - \cancel{\mu^{H_0^1} u} \Big|_{\partial\Omega} + \left(\frac{\partial \mu^{H_0^1}}{\partial x}, \frac{c}{v} u\right)_{L^2(\Omega)}, \tag{87}$$

where the boundary terms cancel due to $\mu^{H_0^1}$ being zero at the boundaries. Furthermore, the remaining term on the left can be identified to be a duality pairing in H_0^1 , which exactly yields the expansion coefficients of the projection ($\mathcal{N}^0(\bar{u})$) as noted in (60).



(a) Exact solution to advection-diffusion equation and its H_0^1 and L^2 projections with $\alpha = 50$



(b) Fine-scales for H_0^1 projection computed using the Fine-Scale Greens' functions (c) Fine-scales for L^2 projection computed using the Fine-Scale Greens' functions

Fig. 18. Mesh with polynomial degree $p = 4$ and 3 elements.

We thus have the following equations for the projection/resolved scales and the fine scales

$$\mathcal{N}^0(\bar{u}) = \left(\mu^{H_0^1}, \frac{1}{v} f \right)_{L^2(\Omega)} + \left(\frac{\partial \mu^{H_0^1}}{\partial x}, \frac{c}{v} (\bar{u} + u') \right)_{L^2(\Omega)} \rightarrow \bar{u} = \psi^{(0)} \mathcal{N}^0(\bar{u}) \tag{88}$$

$$u' = \mathcal{G}' \mathcal{R} \bar{u} = \mathcal{G}' \left(\frac{1}{v} f - \frac{c}{v} \frac{\partial \bar{u}}{\partial x} - \frac{c}{v} \frac{\partial u'}{\partial x} + \frac{\partial^2 \bar{u}}{\partial x^2} \right), \tag{89}$$

where use the fact that $u = \bar{u} + u'$. An important thing to note is that this formulation solves for the strong u' which we choose to represent on a finer mesh.¹ For conciseness, we will use the following shorthand notation to represent the above equations

$$\bar{u} = \bar{\Phi}(f, \bar{u}, u') \tag{90}$$

$$u' = \Phi'(f, \bar{u}, u'). \tag{91}$$

In order to solve this coupled set of equations, we employ an iterative scheme, where we initialise $\bar{u}_0 = 0$ and $u'_0 = 0$, and use the following update equations to compute \bar{u} and u' at the $i + 1$ iteration

$$\bar{u}_{i+1} = \bar{u}_i + w(\bar{\Phi}(f, \bar{u}_i, u'_i) - \bar{u}_i) \tag{92}$$

$$u'_{i+1} = u'_i + w(\Phi'(f, \bar{u}_i, u'_i) - u'_i), \tag{93}$$

¹ The finer mesh is solely used to represent/plot u' .

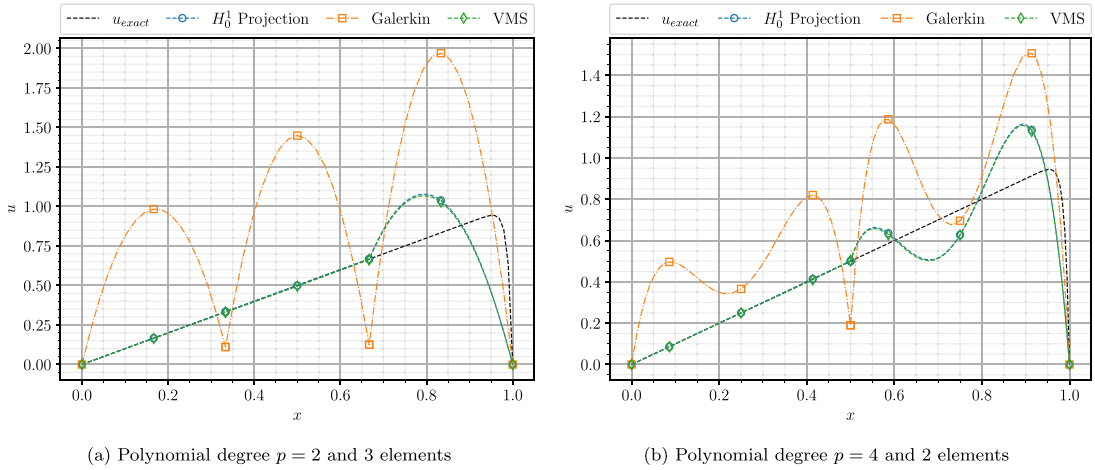


Fig. 19. Exact solution and its H_0^1 projection plotted alongside the Galerkin solution and the iterative VMS approach.

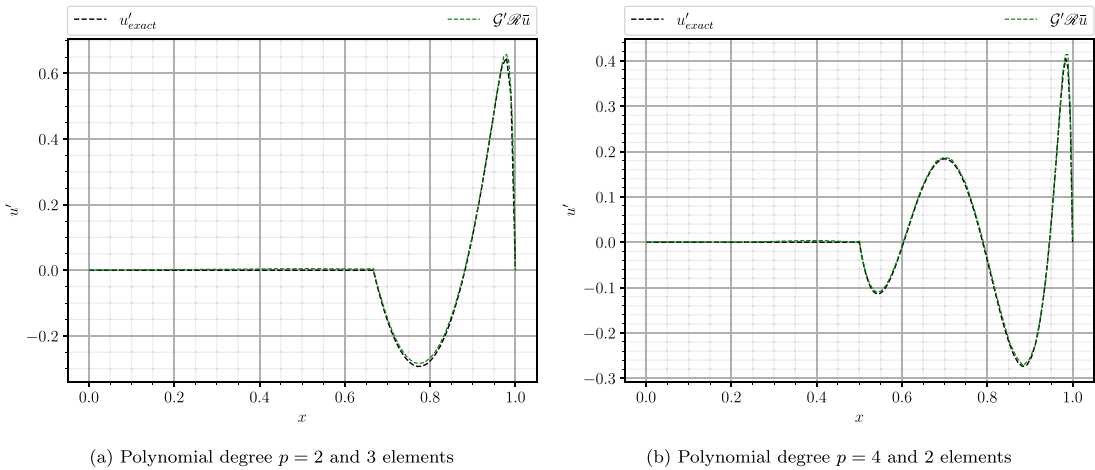


Fig. 20. Exact fine-scales and the fine-scales for the H_0^1 projection computed using the Fine-Scale Greens' function through the iterative approach.

with w as the under-relaxation factor which we set equal to $\frac{1}{2\alpha}$, with α given by (79). We successively iterate the above equations until the residual drops below a user-specified tolerance ϵ , $\|\bar{u}_{i+1} - \bar{u}_i\|_{L^2} < \epsilon$. For all the results shown in this subsection, the tolerance was set to $\epsilon = 10^{-8}$.

The results of this iterative VMS approach are shown in Figs. 19 and 20. Firstly, Fig. 19 shows the exact solution and its H_0^1 projection plotted alongside the Galerkin solution and the newly proposed iterative VMS approach (labelled as 'VMS'). Subsequently, Fig. 20 shows the computed u' alongside the exact fine-scales of the projection. From these results, it is evident that the iterative VMS approach successfully yields, up to integration and iteration error, a numerical solution that is the projection of the exact solution and it further returns the corresponding missing fine scales. It is worth noting that the proposed iterative approach is subject to some amount of numerical error as evident through the small discrepancy between the exact and the iteratively computed fine scales seen in Fig. 20. This error is attributed to the choice of ϵ and the refinement level of the finer mesh where we represent u' (i.e. the degree of precision of the quadrature rule used for (89)).

5. Computing the Fine-Scale Greens' function for 2D problems

We now demonstrate that the aforementioned claim that the Fine-Scale Greens' function can be constructed using dual basis functions naturally extends to multi-dimensional cases. For the sake of demonstration, we limit our focus to the H_0^1 projection and the 2D Poisson equation given by

$$-\nabla \cdot \nabla \phi = f, \quad \mathbf{x} \in \Omega = [0, 1]^2 \tag{94}$$

$$\phi(\mathbf{x}) = 0, \quad \mathbf{x} \in \partial\Omega. \tag{95}$$

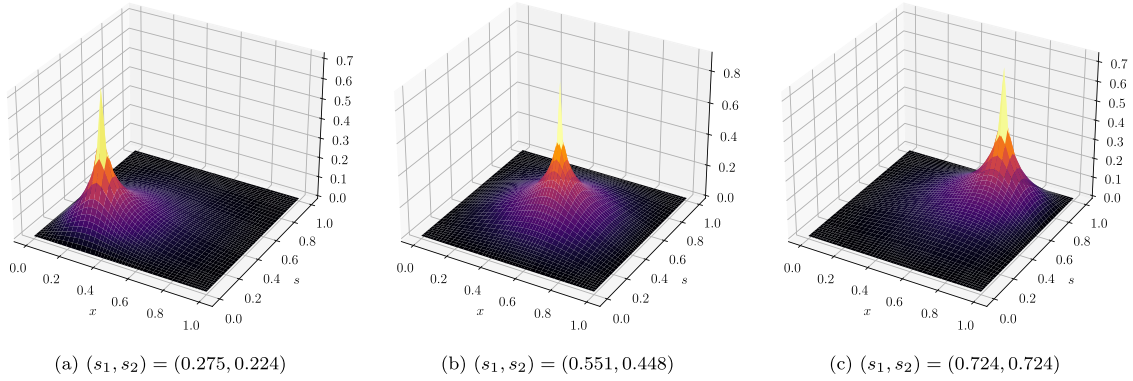


Fig. 21. Truncated Greens' function for 2D Poisson equation at various points in the domain.

The Greens' function associated with this problem may be expressed as an eigenfunction expansion as follows [29]

$$g(\mathbf{x}, \mathbf{s}) = g(x, y, s_1, s_2) = \sum_{n=1}^{\infty} -\frac{(2 \sin(n\pi s_1) \sin(n\pi x))}{(n\pi \sinh(n\pi))} \begin{cases} \sinh(n\pi(s_2 - 1)) \sinh(n\pi y), & y < s_2 \\ \sinh(n\pi(y - 1)) \sinh(n\pi s_2), & y \geq s_2. \end{cases} \quad (96)$$

To derive the H_0^1 dual basis functions for the 2D case, we substitute

$$\bar{\phi} := \tilde{\psi}^{(0)} \tilde{\mathcal{N}}^0(\bar{\phi}) \quad (97)$$

$$-\Delta_h v^h := \tilde{\psi}^{(0)} \tilde{\mathcal{N}}^0(v^h) \iff v^h = (-\Delta_h^{-1} \tilde{\psi}^{(0)}) \tilde{\mathcal{N}}^0(v^h), \quad (98)$$

into (55), which yields

$$\tilde{\mathcal{N}}^0(v^h)^T (-\Delta_h^{-1} \tilde{\psi}^{(0)}, \tilde{\psi}^{(0)})_{H_0^1(\Omega)} \tilde{\mathcal{N}}^0(\bar{\phi}) = \tilde{\mathcal{N}}^0(v^h)^T (-\Delta_h^{-1} \tilde{\psi}^{(0)}, \phi)_{H_0^1(\Omega)}, \quad \forall \tilde{\mathcal{N}}^0(v^h)^T \in \mathbb{R}^n. \quad (99)$$

As for the 1D case, we use the fact that $(-\Delta_h^{-1} \tilde{\psi}^{(0)}, \tilde{\psi}^{(0)})_{H_0^1(\Omega)} = \delta_{i,j}$ which gives

$$\tilde{\mathcal{N}}^0(\bar{\phi}) = (-\Delta_h^{-1} \tilde{\psi}^{(0)}, \phi)_{H_0^1(\Omega)}. \quad (100)$$

Subsequently we define our 2D H_0^1 dual basis functions $\mu^{H_0^1}$ as

$$\mu^{H_0^1} := -\Delta_h^{-1} \tilde{\psi}^{(0)}. \quad (101)$$

Remark 5.1. The 2D H_0^1 dual basis functions are defined using the *dual nodal* functions $\tilde{\psi}^{(0)}$ as opposed to the primal nodal functions used for the 1D case. See Appendix and [30] for details on the construction of the discrete Laplacian operator.

Using these H_0^1 dual basis functions and the Greens' function in (96), we can construct the Fine-Scale Greens' function in the exact same manner as for the 1D case. We choose to truncate the series in (96) to a finite value of 100 terms for practical implementation. The plot of the truncated Greens' function and the corresponding Fine-Scale Greens' function for the H_0^1 projection are visualised in Fig. 21 and Fig. 22 respectively.

5.1. Reconstruction of fine-scale terms of a projection (2D)

We perform similar numerical tests as for the 1D case where we compute the projection of an exact solution to the Poisson problem and reconstruct the fine scales. For this 2D case, we take as the source term

$$f = 8\pi^2 \sin(2\pi x) \sin(2\pi y), \quad (102)$$

which leads to the following exact solution

$$\phi_{exact} = \sin(2\pi x) \sin(2\pi y). \quad (103)$$

The exact solution and its H_0^1 projection onto two different meshes² are shown in Figs. 23 and 25. Subsequently, the exact fine scales and the reconstruction thereof computed using the Fine-Scale Greens' function are shown in Figs. 24 and 26. These plots clearly indicate that the described Fine-Scale Greens' function correctly reproduces the missing unresolved scales of a projection.

² p refers to degree of nodal polynomials, see Remark 3.1

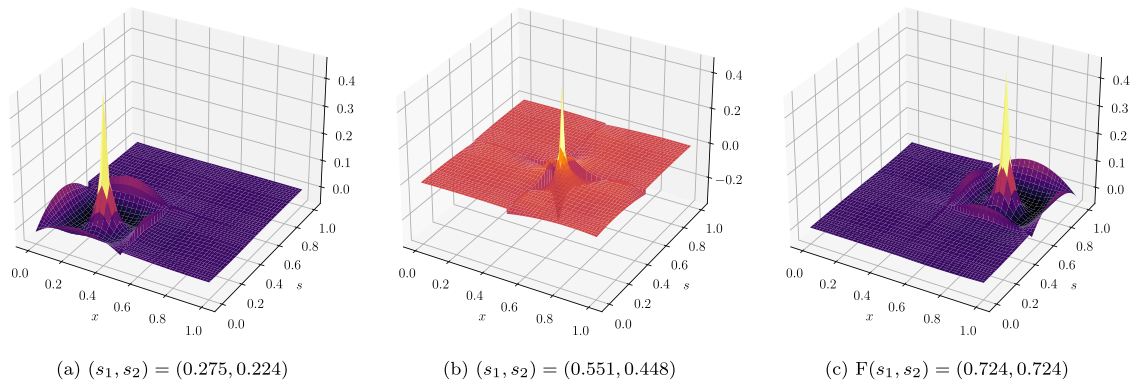


Fig. 22. Fine-Scale Greens' function for 2D Poisson equation at various points in the domain.

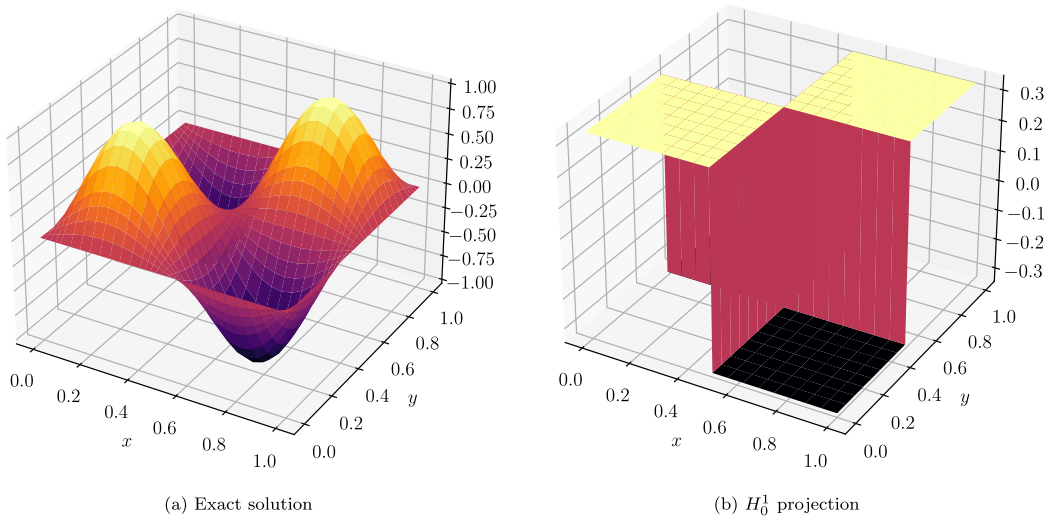


Fig. 23. Exact solution and H_0^1 projection of 2D Poisson equation on a mesh with 2×2 elements with polynomial degree $p = 1$.

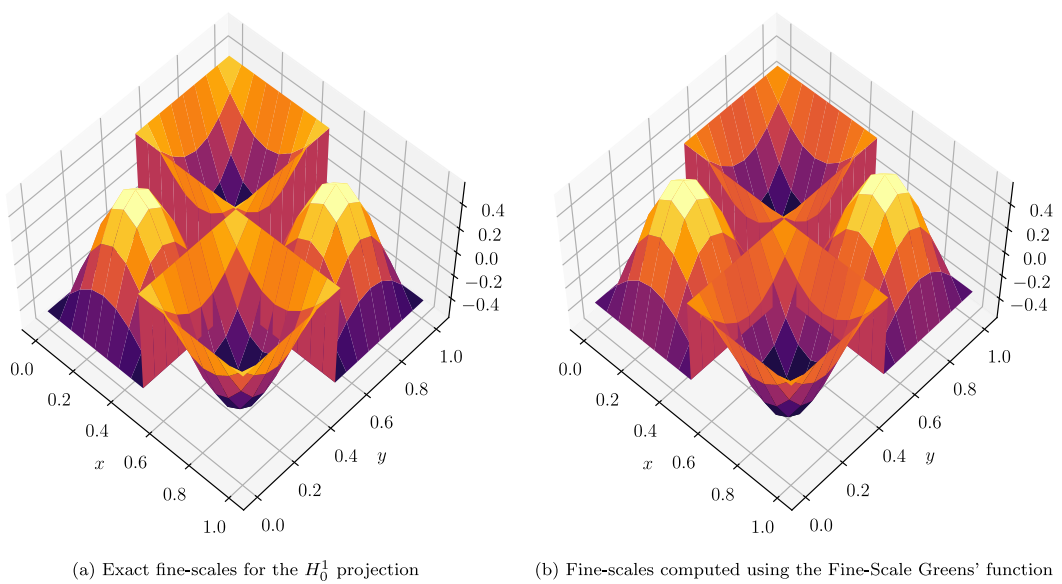


Fig. 24. Unresolved fine-scales of the H_0^1 projection of the 2D Poisson equation on a mesh with 2×2 elements with polynomial degree $p = 1$.

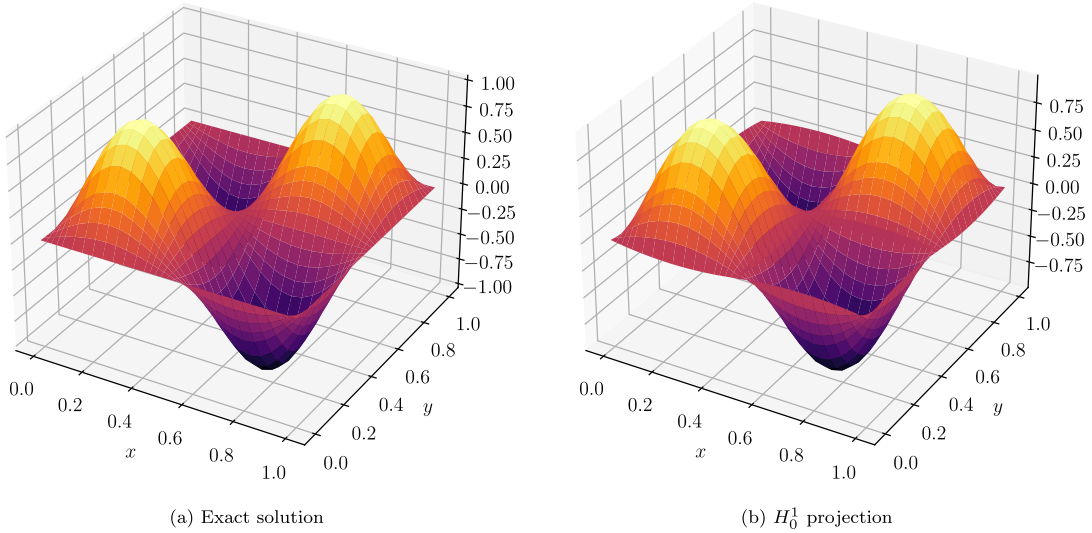


Fig. 25. Exact solution and H_0^1 projection of 2D Poisson equation on a mesh with 2×2 elements with polynomial degree $p = 4$.

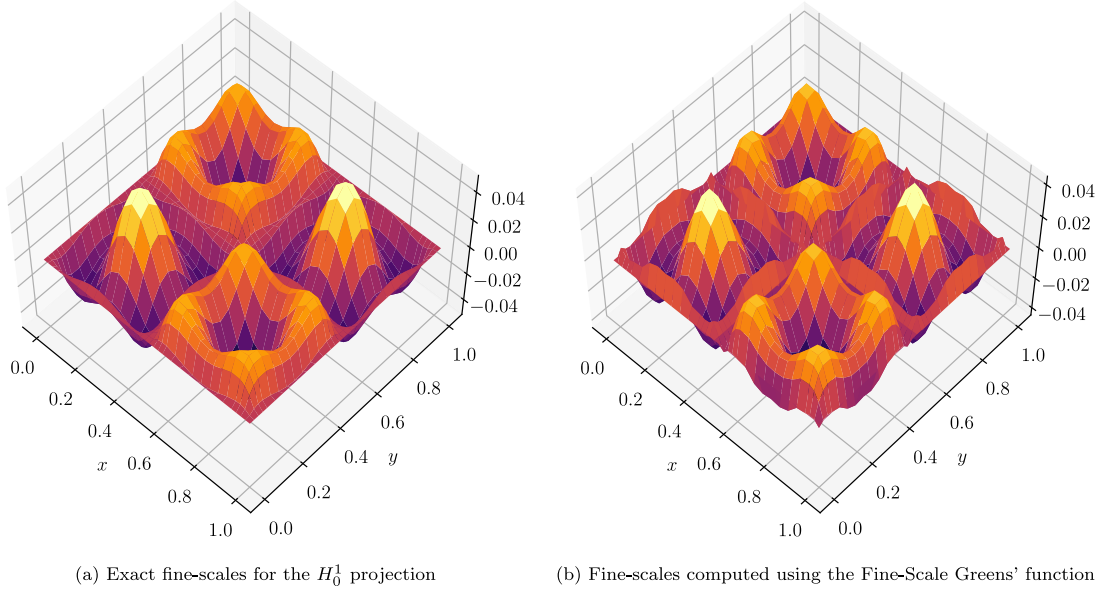


Fig. 26. Unresolved fine-scales of the H_0^1 projection of the 2D Poisson equation on a mesh with 2×2 elements with polynomial degree $p = 4$.

6. Summary

In this paper, we have proposed a new approach for explicitly constructing the Fine-Scale Greens' function by employing the concept of dual basis functions. We have shown that these dual basis functions encode the projector and are explicitly computable thus making them an appropriate choice for the μ 's presented in [25]. Moreover, the constructed Fine-Scale Greens' function is clearly shown to successfully reconstruct all the missing fine scales truncated with the projection. Since the dual basis functions naturally extend to higher dimensions, we have a generalised approach for computing the Fine-Scale Greens' function for any projector in arbitrary dimensions. Furthermore, even though we solely focus on the Fine-Scale Greens' functions for the Poisson equation, we have demonstrated that it may be employed in VMS approaches for other problems such as the steady advection–diffusion problem albeit in a non-monolithic manner. We do remark that while everything we presented was implemented in the context of the MSEM, the concepts of the dual basis may be employed in any other framework to produce an appropriate Fine-Scale Greens' function. Regarding future work, a natural continuation of this paper will be the development of numerical integration rules that accurately and efficiently integrate the Fine-Scale Greens' function. Subsequently, the methodology could be

expanded to address increasingly intricate non-linear problems, such as the Navier–Stokes equations, with consideration given to multi-dimensional advection–diffusion problems as intermediary stages.

CRedit authorship contribution statement

Suyash Shrestha: Writing – review & editing, Writing – original draft, Methodology, Conceptualization. **Joey Dekker:** Writing – review & editing, Writing – original draft, Methodology, Conceptualization. **Marc Gerritsma:** Writing – review & editing, Writing – original draft, Methodology, Conceptualization. **Steven Hulshoff:** Writing – review & editing, Methodology, Conceptualization. **Ido Akkerman:** Writing – review & editing, Methodology, Conceptualization.

Declaration of competing interest

The authors declare that they have no known competing financial interests or personal relationships that could have appeared to influence the work reported in this paper.

Data availability

Data will be made available on request.

Appendix. Discrete Laplacian operator in 2D

In this section, we shall describe the construction of the discrete Laplacian operator used for defining the H_0^1 projection in 2D from Section 5. We start with a Poisson problem defined as follows

$$-\nabla \cdot \nabla \phi = f, \quad \mathbf{x} \in \Omega \quad (\text{A.1})$$

$$\phi(\mathbf{x}) = 0, \quad \mathbf{x} \in \partial\Omega. \quad (\text{A.2})$$

We then rewrite the problem in a mixed formulation by defining a vector field \underline{u} as the gradient of ϕ

$$\underline{u} - \nabla \phi = 0 \quad (\text{A.3})$$

$$-\nabla \cdot \underline{u} = f. \quad (\text{A.4})$$

The Galerkin weak form of this mixed formulation is obtained by testing (A.3) with $\underline{v} \in H(\text{div}, \Omega)$ and (A.4) with $\varphi \in L^2(\Omega)$

$$(\underline{v}, \underline{u})_{L^2(\Omega)} + (\nabla \cdot \underline{v}, \phi)_{L^2(\Omega)} = \int_{\partial\Omega} \phi \underline{v} \cdot \underline{n} \, d\Gamma, \quad \forall \underline{v} \in H(\text{div}, \Omega) \quad (\text{A.5})$$

$$-(\varphi, \nabla \cdot \underline{u})_{L^2(\Omega)} = (\varphi, f)_{L^2(\Omega)}, \quad \forall \varphi \in L^2(\Omega), \quad (\text{A.6})$$

where we have performed integration by parts on the gradient of ϕ and the emerging boundary integral is used to weakly impose the homogeneous Dirichlet boundary condition by setting it to zero. Carrying out this integration by parts is what allows us to eventually perform the H_0^1 projection in a discontinuous space.

An important remark about the choice of function spaces is that they satisfy the De Rham sequence, i.e. applying the divergence to an element of $H(\text{div}, \Omega)$ maps the element to $L^2(\Omega)$

$$H(\text{div}, \Omega) \xrightarrow{\nabla \cdot} L^2(\Omega).$$

This property must also be satisfied at the discrete level when selecting the finite-element subspaces, see [31].

Transforming (A.5) and (A.6) into the discrete setting by expanding ϕ in the space of dual nodal basis functions ($\phi = \tilde{\psi}^{(0)} \phi$) and \underline{u} in (2D) edge basis functions ($\underline{u} = \psi^{(1)} \mathbf{u}$) gives

$$\mathbb{M}^{(1)} \mathbf{u} + \nabla_h^T \cdot \phi = 0 \quad (\text{A.7})$$

$$-\nabla_h \cdot \mathbf{u} = \hat{f}, \quad (\text{A.8})$$

where $\mathbb{M}^{(1)}$ is mass matrix whose entries correspond to the L^2 inner product of the basis functions spanning a subset of $H(\text{div}, \Omega)$ (2D edge basis functions $(\psi_i^{(1)}, \psi_j^{(1)})_{L^2(\Omega)}$), $\nabla_h \cdot$ is the discrete divergence operator, and \mathbf{u} and ϕ are the degrees of freedom. Given the invertibility of $\mathbb{M}^{(1)}$, [26], we rearrange (A.7) to get an expression for \mathbf{u} as follows

$$\mathbf{u} = -\mathbb{M}^{(1)-1} \nabla_h^T \cdot \phi, \quad (\text{A.9})$$

which we plug into (A.8) to get

$$\nabla_h \cdot \mathbb{M}^{(1)-1} \nabla_h^T \cdot \phi = \hat{f}. \quad (\text{A.10})$$

Hence, the discrete operator for the negative Laplacian is given as

$$-\Delta_h = \nabla_h \cdot \mathbb{M}^{(1)-1} \nabla_h^T. \quad (\text{A.11})$$

References

- [1] T. Hughes, L. Franca, M. Mallet, A new finite element formulation for computational fluid dynamics: I. Symmetric forms of the compressible Euler and Navier-Stokes equations and the second law of thermodynamics, *Comput. Methods Appl. Mech. Engrg.* 54 (2) (1986) 223–234, [http://dx.doi.org/10.1016/0045-7825\(86\)90127-1](http://dx.doi.org/10.1016/0045-7825(86)90127-1).
- [2] T. Hughes, M. Mallet, M. Akira, A new finite element formulation for computational fluid dynamics: II. Beyond SUPG, *Comput. Methods Appl. Mech. Engrg.* 54 (3) (1986) 341–355, [http://dx.doi.org/10.1016/0045-7825\(86\)90110-6](http://dx.doi.org/10.1016/0045-7825(86)90110-6).
- [3] T. Hughes, M. Mallet, A new finite element formulation for computational fluid dynamics: III. The generalized streamline operator for multidimensional advective-diffusive systems, *Comput. Methods Appl. Mech. Engrg.* 58 (3) (1986) 305–328, [http://dx.doi.org/10.1016/0045-7825\(86\)90152-0](http://dx.doi.org/10.1016/0045-7825(86)90152-0).
- [4] T. Hughes, M. Mallet, A new finite element formulation for computational fluid dynamics: IV. A discontinuity-capturing operator for multidimensional advective-diffusive systems, *Comput. Methods Appl. Mech. Engrg.* 58 (3) (1986) 329–336, [http://dx.doi.org/10.1016/0045-7825\(86\)90153-2](http://dx.doi.org/10.1016/0045-7825(86)90153-2).
- [5] T. Hughes, L. Franca, M. Balestra, A new finite element formulation for computational fluid dynamics: V. Circumventing the Babuška-Brezzi condition: A stable Petrov-Galerkin formulation of the Stokes problem accommodating equal-order interpolations, *Comput. Methods Appl. Mech. Engrg.* 59 (1) (1986) 85–99, [http://dx.doi.org/10.1016/0045-7825\(86\)90025-3](http://dx.doi.org/10.1016/0045-7825(86)90025-3).
- [6] T. Hughes, L.P. Franca, M. Mallet, A new finite element formulation for computational fluid dynamics: VI. Convergence analysis of the generalized SUPG formulation for linear time-dependent multidimensional advective-diffusive systems, *Comput. Methods Appl. Mech. Engrg.* 63 (1) (1987) 97–112, [http://dx.doi.org/10.1016/0045-7825\(87\)90125-3](http://dx.doi.org/10.1016/0045-7825(87)90125-3).
- [7] T. Hughes, L. Franca, A new finite element formulation for computational fluid dynamics: VII. The Stokes problem with various well-posed boundary conditions: Symmetric formulations that converge for all velocity/pressure spaces, *Comput. Methods Appl. Mech. Engrg.* 65 (1) (1987) 85–96, [http://dx.doi.org/10.1016/0045-7825\(87\)90184-8](http://dx.doi.org/10.1016/0045-7825(87)90184-8).
- [8] T. Hughes, L. Franca, G. Hulbert, A new finite element formulation for computational fluid dynamics: VIII. The Galerkin/least-squares method for advective-diffusive equations, *Comput. Methods Appl. Mech. Engrg.* 73 (2) (1989) 173–189, [http://dx.doi.org/10.1016/0045-7825\(89\)90111-4](http://dx.doi.org/10.1016/0045-7825(89)90111-4).
- [9] F. Shakib, T. Hughes, A new finite element formulation for computational fluid dynamics: IX. Fourier analysis of space-time Galerkin/least-squares algorithms, *Comput. Methods Appl. Mech. Engrg.* 87 (1) (1991) 35–58, [http://dx.doi.org/10.1016/0045-7825\(91\)90145-V](http://dx.doi.org/10.1016/0045-7825(91)90145-V).
- [10] F. Shakib, T. Hughes, Z. Johan, A new finite element formulation for computational fluid dynamics: X. The compressible Euler and Navier-Stokes equations, *Comput. Methods Appl. Mech. Engrg.* 89 (1) (1991) 141–219, [http://dx.doi.org/10.1016/0045-7825\(91\)90041-4](http://dx.doi.org/10.1016/0045-7825(91)90041-4), Second World Congress on Computational Mechanics.
- [11] S. Farzin, *Finite Element Analysis Of The Compressible Euler And Navier-Stokes Equations* (Ph.D. thesis), Stanford University, 1988.
- [12] T. Hughes, Multiscale phenomena: Green's functions, the Dirichlet-to-Neumann formulation, subgrid scale models, bubbles and the origins of stabilized methods, *Comput. Methods Appl. Mech. Engrg.* 127 (1–4) (1995) 387–401, [http://dx.doi.org/10.1016/0045-7825\(95\)00844-9](http://dx.doi.org/10.1016/0045-7825(95)00844-9).
- [13] E. Munts, S. Hulshoff, R. de Borst, A space-time variational multiscale discretization for Les, in: 34th AIAA Fluid Dynamics Conference and Exhibit, 2004, <http://dx.doi.org/10.2514/6.2004-2132>.
- [14] Y. Bazilevs, V. Calo, Y. Zhang, T. Hughes, Isogeometric fluid–structure interaction analysis with applications to arterial blood flow, *Comput. Mech.* 38 (4–5) (2006) 310–322, <http://dx.doi.org/10.1007/s00466-006-0084-3>.
- [15] Y. Bazilevs, V. Calo, J. Cottrell, T. Hughes, A. Reali, G. Scovazzi, Variational multiscale residual-based turbulence modeling for large eddy simulation of incompressible flows, *Comput. Methods Appl. Mech. Engrg.* 197 (1–4) (2007) 173–201, <http://dx.doi.org/10.1016/j.cma.2007.07.016>.
- [16] L. Holmen, T. Hughes, A. Oberai, G. Wells, Sensitivity of the scale partition for variational multiscale large-eddy simulation of channel flow, *Phys. Fluids* 16 (3) (2004) 824–827, <http://dx.doi.org/10.1063/1.1644573>.
- [17] T. Hughes, L. Mazzei, A. Oberai, A. Wray, The multiscale formulation of large eddy simulation: Decay of homogeneous isotropic turbulence, *Phys. Fluids* 13 (2) (2001) 505–512, <http://dx.doi.org/10.1063/1.1332391>.
- [18] S.K. Stoter, S.R. Turteltaub, S.J. Hulshoff, D. Schilling, Residual-based variational multiscale modeling in a discontinuous Galerkin framework, *Multiscale Model Simul* 16 (3) (2018) 1333–1364, <http://dx.doi.org/10.1137/17m1147044>.
- [19] J. Bazilevs, *Isogeometric Analysis of Turbulence and Fluid-Structure Interaction* (Ph.D. thesis), The University of Texas at Austin, 2006.
- [20] B. Koobus, C. Farhat, A variational multiscale method for the large eddy simulation of compressible turbulent flows on unstructured meshes—application to vortex shedding, *Comput. Methods Appl. Mech. Engrg.* 193 (15–16) (2004) 1367–1383, <http://dx.doi.org/10.1016/j.cma.2003.12.028>.
- [21] V. Levasseur, P. Sagaut, F. Chalot, A. Davroux, An entropy-variable-based VMS/GLS method for the simulation of compressible flows on unstructured grids, *Comput. Methods Appl. Mech. Engrg.* 195 (9–12) (2006) 1154–1179, <http://dx.doi.org/10.1016/j.cma.2005.04.009>.
- [22] M. ten Eikelder, I. Akkerman, Correct energy evolution of stabilized formulations: The relation between VMS, SUPG and GLS via dynamic orthogonal small-scales and isogeometric analysis. I: The convective–diffusive context, *Comput. Methods Appl. Mech. Engrg.* 331 (2018) 259–280, <http://dx.doi.org/10.1016/j.cma.2017.11.020>.
- [23] M. ten Eikelder, Y. Bazilevs, I. Akkerman, A theoretical framework for discontinuity capturing: Joining variational multiscale analysis and variation entropy theory, *Comput. Methods Appl. Mech. Engrg.* 359 (2020) 112664, <http://dx.doi.org/10.1016/j.cma.2019.112664>.
- [24] T. Hughes, G. Feijóo, L. Mazzei, J. Quincy, The variational multiscale method—a paradigm for computational mechanics, *Comput. Methods Appl. Mech. Eng.* 166 (1–2) (1998) 3–24, [http://dx.doi.org/10.1016/S0045-7825\(98\)00079-6](http://dx.doi.org/10.1016/S0045-7825(98)00079-6).
- [25] T. Hughes, G. Sangalli, Variational multiscale analysis: The fine-scale green's function, projection, optimization, localization, and stabilized methods, *SIAM J. Numer. Anal.* 45 (2) (2007) 539–557, <http://dx.doi.org/10.1137/050645646>.
- [26] V. Jain, Y. Zhang, A. Palha, M. Gerritsma, Construction and application of algebraic dual polynomial representations for finite element methods on quadrilateral and hexahedral meshes, *Comput. Math. Appl.* 95 (2021) 101–142, <http://dx.doi.org/10.1016/j.camwa.2020.09.022>.
- [27] M. Gerritsma, Edge functions for spectral element methods, in: *Lecture Notes in Computational Science and Engineering*, 2010, pp. 199–207, <http://dx.doi.org/10.1007/978-3-642-15337-2-17>.
- [28] T. Frankel, *The Geometry of Physics: An Introduction*, Cambridge University Press, 2011.
- [29] R. Haberman, *Applied Partial Differential Equations with Fourier Series and Boundary Value Problems*, Pearson, 2019.
- [30] Y. Zhang, V. Jain, A. Palha, M. Gerritsma, A high order hybrid mimetic discretization on curvilinear quadrilateral meshes for complex geometries, in: *European Conference on Computational Fluid Dynamics*, 2018.
- [31] D. Arnold, R. Falk, R. Winther, Finite element exterior calculus: From Hodge theory to numerical stability, *Bull. Amer. Math. Soc.* 47 (2) (2010) 281–354, <http://dx.doi.org/10.1090/S0273-0979-10-01278-4>.